Nanoscale

ROYAL SOCIETY OF CHEMISTRY

REVIEW

View Article Online
View Journal | View Issue

Cite this: *Nanoscale*, 2024, **16**, 9259

Emerging trends in metal oxide-based electronic noses for healthcare applications: a review

Zain Ul Abideen, *†[a] Waqas Ul Arifeen †[b] and Y. M. Nuwan D. Y. Bandara[a]

Received 6th January 2024,
Accepted 20th April 2024

DOI: 10.1039/d4nr00073k

rsc.li/nanoscale

An electronic nose (E-nose) is a technology fundamentally inspired by the human nose, designed to detect, recognize, and differentiate specific odors or volatile components in complex and chaotic environments. Comprising an array of sensors with meticulously designed nanostructured architectures, E-noses translate the chemical information captured by these sensors into useful metrics using complex pattern recognition algorithms. E-noses can significantly enhance the quality of life by offering preventive point-of-care devices for medical diagnostics through breath analysis, and by monitoring and tracking hazardous and toxic gases in the environment. They are increasingly being used in defense and surveillance, medical diagnostics, agriculture, environmental monitoring, and product validation and authentication. The major challenge in developing a reliable E-nose involves miniaturization and low power consumption. Various sensing materials are employed to address these issues. This review presents the key advancements over the last decade in E-nose technology, specifically focusing on chemiresistive metal oxide sensing materials. It discusses their sensing mechanisms, integration into portable E-noses, and various data analysis techniques. Additionally, we review the primary metal oxide-based E-noses for disease detection through breath analysis. Finally, we address the major challenges and issues in developing and implementing a portable metal oxide-based E-nose.

[a]*Nanotechnology Research Laboratory, Research School of Chemistry, College of Science, Australian National University, Canberra, ACT, 2601, Australia. E-mail: zainulabideen@anu.edu.au*
[b]*School of Mechanical Engineering, Yeungnam University, Daehak-ro, Gyeongsan-si, Gyeongbuk-do, 38541, South Korea*
† These authors contributed equally to this work.

1 Introduction

Metal oxide semiconductors (MOS) are commonly used for the fabrication of solid-state gas sensors, which deliver conspicuous performance compared to other types of gas sensing

Zain Ul Abideen

Zain Ul Abideen, a recent PhD candidate at ANU's College of Engineering and Computer Science, has submitted his thesis on flame synthesized metal oxide nanoparticles and opto-electronic devices for gas sensing. His research, part of the OHIOH initiative, was directed towards evolving personalized medical technology. With prior experience as a Product Development Engineer in South Korea, he has a robust background in inorganic nanomaterials for advanced applications. Zain holds a Master's degree from Inha University, Republic of Korea, focusing on nanocomposite gas sensors, and a Bachelor's in Materials Engineering from GIK Institute, Pakistan.

Waqas Ul Arifeen

Waqas Ul Arifeen received his bachelor's degree in Industrial & Manufacturing Engineering from UET Lahore in 2015. He earned his Ph.D. degree in Mechanical Engineering in 2020 from Yeungnam University under the supervision of Professor Tae Jo Ko. He is currently an Assistant Professor at Yeungnam University, South Korea. His research interests focus on the design, synthesis, and physico-electrochemical characterization of solid-state electrolytes and separators for lithium-ion batteries.

technologies. Chemiresistive sensors using MOS are sought after for several reasons, including their sensitivity, low manufacturing cost, lightweight, and small form factor, which are ideal for portable devices. They are widely used in environmental monitoring, indoor air quality monitoring (*e.g.*, for carbon monoxide, oxygen, carbondioxide sensors), and safety applications (*e.g.*, detection of volatile organic compounds (VOCs), toxic gases, and leaks).[1,2] However, despite their widespread adoption across a broad spectrum of applications, their lack of antibody-like high-precision selectivity for target gases has hindered their advancement in more demanding commercial spaces, particularly in point-of-care applications.[3,4]

With miniaturized devices gaining considerable traction over the last few decades due to advancements in micro-electronics and nano-fabrication, the beneficial aspects of prominent sensors for gas-detection applications have shown tremendous potential for integration into such devices for sample-to-answer applications and beyond.[5–7] Moreover, such research efforts invariably require solutions to address the core legacy shortcomings of gas sensors (*vide-infra*), which is essential for high-precision applications (*e.g.*, medical devices). Although most sensors have been shown to work in controlled environments (*i.e.*, laboratory conditions), the true test of their efficacy lies in their performance in more chaotic environments with impurities and competing gases (*i.e.*, real-world applications).

The response of a sensor to a target gas (R_{sensor}) is generally represented by the ratio of its resistance in the presence of the target gas (R_g) to its baseline resistance in target-gas-free air (R_{air}): $R_{sensor} = R_g/R_{air} - 1$. Thus, depending on the values of R_g and R_{air}, R_{sensor} could be greater or less than 1. This inequality largely depends on the characteristics of the target gas and the MOS-based sensing layer. To this extent, gases are broadly categorized into two classes: oxidizing ($R_g > R_{air}$) and reducing gases ($R_g < R_{air}$).[8,9]

Numerous gases can be identified using a single substrate/sensor, addressing a persistent problem of limited selectivity with many MOS-based sensing materials. Efforts are underway to enhance selectivity towards specific target gases, thereby reducing responsiveness to non-target gases.[10] While developing sensors with true antibody-like selectivity to a target gas may not be straightforward, an array of sensors with partial selectivity, mimicking animal olfactory receptors, could be the key to gas identification efforts, as discussed in this review. These devices are termed electronic noses (E-noses), as they simulate the functioning of animal noses.

In animals, responses from non-selective or partially selective receptors are combined and processed to develop, and by extension, associate typical patterns with different volatile compounds, similar to pattern recognition using machine learning.[11] Similarly, an E-nose, which is a synthetic nose comprising an array of sensors, can recognize different gases and estimate their concentrations through the patterns generated by its sensors' responses to target gases.[9,12] An E-nose essentially consists of a chemical sensor array, electronic circuit, and data analysis software. Despite the high customizability of these components, integrating the hardware into a single, portable device with a low form factor remains challenging but is often demanded by modern consumer economics.[13]

Advancements in nano-fabrication, materials science, and micro-electronics have paved the way for the development of technologies that mimic fundamental sensory receptors of the biological world, enabling the detection of stimulations beyond the capabilities of their natural counterparts. These technologies have found applications in defense and surveillance,[14] medical diagnostics,[15] agriculture,[15,16] environmental monitoring, and product validation and authentication. E-noses have applications spanning commercial, security, food, and health sectors, which are crucial for leveraging such promising advancements in sensor technologies. With the rich availability of resources and rapid progress in these fields, there is a significant drive towards developing small, portable, and affordable E-noses.

These developments are particularly impactful in healthcare, where they offer novel approaches to disease diagnosis and monitoring by detecting specific VOCs indicative of various health conditions. As mentioned earlier, the E-nose comprises multiple sensors, each generating distinct characteristics when exposed to the volatiles emitted by the analyte, thereby creating a unique pattern that is processed by a single system. Although complete selectivity for each volatile is ideal, in practice, achieving high selectivity remains a goal. Chemiresistive sensors are particularly well-suited for integration into E-noses due to their simple electrical characteristics and straightforward interface circuitry, facilitating easier integrated circuit (IC) integration.[16]

In this context, this review will explore recent developments in MOS-based E-nose systems, including the fabrication techniques for MOS sensors, the transduction principles

Y. M. Nuwan D. Y. Bandara

*Dr Nuwan Bandara graduated from the University of Rhode Island (USA) in 2018 with a Ph.D. in chemistry. His Ph.D. work mainly focused on nanopore-based single-molecule sensing and surface chemical modifications for optical and electrical sensing. His postdoctoral work was initially focused on further exploring the nanopore-based characterization of a host of biomolecules (*e.g.*, proteins) and bioparticles (*e.g.*, viruses) using both planar nanopores and nanopipettes. Currently, he is working as a Research Fellow at The Australian National University developing custom electronics to measure readouts from sensors aimed to detect breath acetone—a biomarker for diabetes—and nanopore-based single molecule sensing.*

employed, and their advantages in health applications. Furthermore, it will delve into a diverse range of healthcare applications where these E-nose systems have demonstrated potential. Finally, the review will discuss the current challenges associated with these systems, along with prospects and potential avenues for further research. By critically analyzing recent advancements in MOS-based E-noses for health applications, this review intends to provide valuable insights into the current state-of-the-art techniques, identify areas for improvement, and inspire further research and development in this promising field.

2 Electronic nose systems: an overview

To address the inherent limitations in the selectivity of chemiresistive MOS-based sensors, considerable efforts have been made to develop an array of sensors, also termed an E-nose. As previously mentioned, an E-nose mimics the mammalian olfactory system by filtering and reacting with VOCs, amplifying signal responses, and recognizing these VOCs. Machine learning (ML) and artificial intelligence (AI) implementations are then employed to analyze the key components of the data.[17] Persaud and Dodd were pioneers in this field, developing the first reported E-nose for odor discrimination. They achieved differentiation among various VOCs by simulating the olfactory system with three commercially available MOS-based gas sensors. Like the mammalian olfactory system, the E-nose is designed to be highly sensitive and selective towards a wide variety of gases.

The olfactory system utilizes feature detection *via* trained receptor cells.[18] Similarly, an E-nose distinguishes between different smells by employing a system that leverages feature extraction or pattern recognition techniques. Recent studies have demonstrated that selective differentiation of VOCs using an E-nose is feasible.[19–23] A schematic illustration of a gas sensing system utilizing an E-nose is shown in Fig. 1.

An E-nose consists of four main components: a sensor array, electronic circuits, data acquisition systems, and a data analysis program.[17,24] The chemical sensor array, the most crucial part of the E-nose, comprises cross-reactive sensing elements. This cross-reactive approach, where each sensor reacts differently to various analytes in a mixture, is similar to how mammalian olfactory systems operate.[22,25] This method generates analyte-specific response patterns by combining the responses from the array elements, thereby enhancing the ability to detect a broader range of analytes as opposed to single sensors developed for high specificity towards a particular biomarker.

Each sensor in the array should detect all or part of the analyte mixture. To achieve this, it is vital to determine each sensing element's characteristics to detect the most significant analyte in a mixture or in the presence of interfering gases. For optimal E-nose performance and cost efficiency, gas sensors should be highly sensitive, precise, quick to recover, repeatable, and stable across different climates or conditions. Various types of sensors have met these criteria in different E-nose systems, including optical, electrochemical, catalytic field-effect, surface acoustic wave, conducting polymers, calorimetric, quartz crystal microbalance, and chemiresistive sensors.[26–28]

Initially, artificial analyte mixtures are used to test the discerning capabilities of sensor arrays before they are used with human breath samples. The unique response patterns to each analyte help establish a relationship between the sensors' sensitivity and selectivity.[29] Although a sensor array or an E-nose might show less sensitivity to a specific analyte compared to a dedicated sensor, its versatility in detecting diverse compounds under various conditions significantly enhances its overall selectivity. If properly configured for cross-reactivity, a sensor array with minimal elements can effectively identify and differentiate multiple analytes. However, a significant challenge for portable E-nose development remains achieving compactness and low power consumption.

3 Data acquisition and analysis techniques for E-nose systems

The analysis of data obtained from E-nose systems is crucial in the development of these devices. It involves several key steps: dimensionality reduction, exploratory data analysis, classification, clustering, and the development of models or algorithms to interpret the outputs.[30–32] A general block diagram illustrating these steps is presented in Fig. 2.

Machine learning (ML) is employed to refine existing algorithms or develop new ones that can detect patterns within data

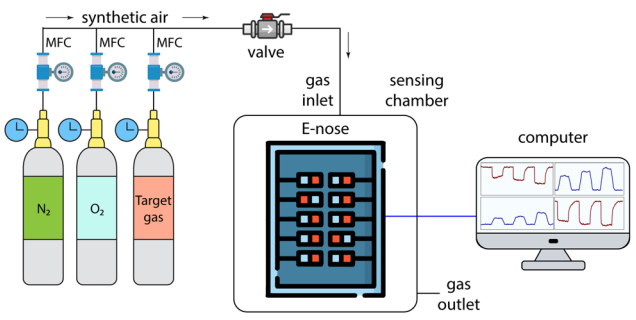

Fig. 1 Schematic illustration of a simple gas sensing setup for an E-nose system.

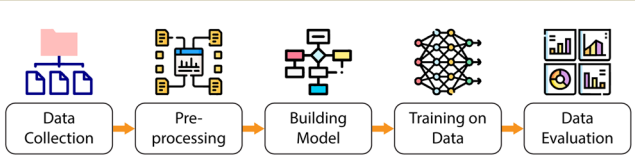

Fig. 2 Steps involved in the data analysis of an E-nose using machine learning algorithms.

and use these insights to predict future trends.[33] The characteristics of an ideal algorithm include robustness, ease of training, low computational power consumption, minimal memory requirements, and high accuracy. ML-based algorithms, such as neural networks, particularly back-propagation neural networks, are relatively simple to implement (the algorithm parameters do not require adjustment during execution) and can be used for both quantitative and qualitative analysis.[11,34]

Statistical approaches such as principal component analysis (PCA), hierarchical cluster analysis (HCA), principal component regression (PCR), discriminant factor analysis (DFA), partial least squares (PLS), and analysis of variance between groups (ANOVA) are generally straightforward to implement.[32] However, their application in broad classifications or predictive modeling can be challenging due to their sensitivity to data variability. Notably, some methods like PCA are often essential for effective ML implementations as they can enhance model performance. With increasing volumes of gas sensing data from multiple sensors, training techniques such as artificial neural networks (ANNs), k-nearest neighbor (KNN), support vector machine (SVM), random forest (RF), fuzzy logic and rules-based algorithms, and genetic algorithms (GA) become critical. These techniques primarily fall within supervised or unsupervised learning categories and are key in generating more precise patterns.[11,30]

Table 1 lists common data analysis methods used for an E-nose equipped with chemiresistive MOS sensors, detailing their advantages and disadvantages.[13] The performance of deep learning algorithms improves with larger datasets, becoming more accurate than classical learning algorithms.[35] Recently, a random forest model trained on features extracted from sensing data proved to be highly effective for analyzing time series data of very similar food samples. The data, derived from a sensor array of 20 single-walled carbon nanotube-based chemiresistive sensors, enabled the model to distinguish between samples of cheese, liquor, and edible oils with up to 91% accuracy, based on their complex odors.[36]

To prevent misdetection and the generation of false patterns, it is crucial to comparatively study and evaluate various ML algorithms and models. This comparison helps to standardize the selection criteria for developing an appropriate pattern recognition system that can accurately detect lower concentrations of analytes.[37] Xu *et al.*[38] assessed three ML algorithms, including a back-propagation neural network, a radial basis function neural network, and support vector regression, for the sub-ppm level detection and prediction of formaldehyde using an E-nose system. The back-propagation neural network was found to be the most accurate for detecting and predicting formaldehyde concentrations in both heavily and lightly polluted air quality conditions. In contrast, the radial basis function neural network exhibited the lowest accuracy, with a mean absolute percentage error of 0.18 for <1 ppm and 0.13 for >1 ppm concentrations of formaldehyde.[38] High detection precision can be achieved through the combination of ML algorithms, and further research is needed in this area.

Sensor drift is another known issue in chemiresistive-based sensors that affects their reliability. This problem is attributed to factors such as sensor aging,[39] environmental changes in temperature and humidity,[40,41] variations in flow rate, and thermo-mechanical degradation.[42] While sensor drift can pose challenges, it does not necessarily render initial statistical models or odor recognition ineffective. However, their efficiency may be compromised under conditions like temperature variations, high humidity levels, long-term use or aging, cross-sensitivity to non-target gases, and the influence of background gases.

To mitigate system inaccuracies, frequent recalibrations are necessary, which can be laborious and costly when involving multiple sensors. Several ML algorithms and signal processing techniques have been developed for drift compensation and recalibration of E-noses.[43–46] Additionally, improvements in sensor stability over time have been achieved through advancements in sensor technology, design, and operational modes.[47–50] A knowledge-adaption-based ML approach has

Table 1 Data analysis methods for MOS sensors-based E-nose systems

Data analysis method	Advantages	Disadvantages	Training speed	Demand for data	Robustness for noise
PCA	Established for pattern visualization	Unsuitable for large data, requires standardization	Fast	Low	Moderate
ANNs	Suits large, non-linear data; fast predictions	Hardware dependent; risk of overfitting	Slow	High	Moderate
Discriminant analysis	Simple implementation, fast classification	Time-consuming training; assumes Gaussian distribution	Moderate	Low	Moderate
Regression	Adaptable, for linear and nonlinear data	Risk of overfitting; poor on small datasets	Fast	Moderate	Moderate
RF	Effective for large, high-dimensional data; handles missing values	Risk of overfitting; computationally intense	Moderate	High	High
KNN	Simple, no data distribution assumption	Expensive with large datasets; sensitive to irrelevant features	Fast	High	High
SVM	High-dimensional effectiveness; clear margin benefits	Full labeling required; poor with large, noisy data	Moderate	Low	Low

also been proposed specifically for drift compensation in E-nose systems.[51]

When high accuracy is essential, deep learning is employed to analyze E-nose responses. This form of ML, which utilizes multiple processing layers to extract features from data, can automatically classify the desired information in new datasets.[52] Deep convolutional recurrent neural network-based algorithms have proven effective, achieving fast gas detection (within 4 seconds) with an accuracy of 98.28%.[53] Deep learning methods are particularly valuable when E-nose systems experience sensor drift, as they help avoid misclassification of odors.[54] However, these methods require high-performance sensors that offer stability and reproducibility to generate large volumes of reliable data.

4 Development of MOS-based E-nose systems

Over the past decade, researchers have actively explored the application of chemiresistive MOS nanostructures, including nanowires,[8] nanotubes,[55] and nanofibers,[56] in the development of compact E-nose systems. Advancements in manufacturing technology have facilitated the integration of MOS nanostructures into microsensor chips, significantly reducing the size and power consumption of these systems.[57] Furthermore, MOS arrays can be engineered for enhanced selectivity by incorporating metal additives and ion implantation, and microsensor arrays with temperature control have been developed for the non-invasive detection of disease biomarkers in clinical diagnostics.

Efforts continue to improve gas sensitivity through the development of MOS-based microarrays. The creation of individual MOS sensors with specific characteristics such as selectivity, reliability, stability, repeatability, and reversibility is crucial for their application in sensor arrays.[58–60] Although there are various methods for designing multiple sensor arrays, using a single set of sensors made from the same material can be cost-effective. However, this approach may limit the ability to analyze multiple gases using vector signals due to the similarity of the sensors within the array.[19]

Various methods have been employed to enhance the selectivity of single-material sensors. One such approach involves utilizing thermal fingerprints and morphological differences between materials. By exploiting the unique response of gas-sensing materials to different noxious gases at specific temperatures, Tonezzer *et al.* developed NiO nanowire-based gas sensors through hydrothermal synthesis.[20] The interdigitated electrodes (IDEs) used in their study consisted of 18 pairs of interdigitated fingers with a spacing of 50 μm, made of Pt/Ti. After calcination at 500 °C for 2 hours, the gas sensing characteristics were observed at different temperatures, and the responses to eight noxious gases including H_2S, NO_2, CO, NH_3, C_2H_5OH, H_2, CO_2, and LPG were investigated. These responses served as specific thermal fingerprints, dependent on the gas concentration and the operating temperature, indicating improved selectivity of the MOS-based chemiresistive gas sensors. The sensing data was used to perform principal component analysis (PCA) of the five patterns with different tendencies output from the asymmetric heater of the fabricated NiO nano sensor, and the variance of PC1, PC2, and PC3 were 81.3%, 148%, and 3.7% (99.8% in total).[20]

In another approach, the successful implementation of SnO_2 nanowires as sensing elements in an electronic micronose, utilizing a gradient gas sensor microarray, was achieved by using percolating SnO_2 nanowire sensing elements.[63] These new sensing elements offered several advantages over traditional nanowires. These nanowire mats exhibited high gas permeability and remained consistent even when the nanowire diameter was reduced. This decoupling of gas permeability from the size of the sensing element's building block was crucial for enhancing the temporal characteristics of the E-nose. Furthermore, nanowire mats possessed a dual signal transduction mechanism, based on the nodes and straight parts of the nanowires.[63]

Sysoev *et al.* utilized the *KAMINA* platform to enhance the sensor's selectivity.[61,62,64] This involved incorporating two Pt thermal resistors on the chip's front side and four heaters on the rear side to distribute the operating temperature evenly across the substrate. A multi-electrode design allowed the gas-sensing MOS thin film to be divided into sensor arrays comprising up to 38 chemical resistors or sensor segments. The synthesis process involved ion beam-assisted chemical deposition, activated by precursor molecules adsorbed from phenyl-tri ethoxy-silane. The spatial non-uniformity in the deposition rate of the silica coating, caused by the density of the Ar^+ beam varying with the distance between the shadow mask opening and the target substrate, resulted in a non-linear variation in coating thickness along the substrate surface, as depicted in Fig. 3a–c.

In another study, they developed a microarray E-nose using a SnO_2 nanowire-based system on the *KAMINA* platform.[63] They controlled the surface temperature of the film with four Pt heaters on the substrate's rear side and exploited variations in the thickness of the gas permeable coating covering the MOS layer to differentiate the responses of the gas sensing material. The gas sensing materials consisted of percolating nanowires with average diameters ranging from 50 to 500 nm and lengths from tens to hundreds of micrometers, forming a dense percolating network. Although some nanowires bridged the 70 μm gap between the electrodes, most contributed to the network. Linear discriminant analysis (LDA) was employed to quantitatively assess the discriminant power of the E-nose.

The findings reveal that a range of VOCs generate a unique signal pattern when detected by the sensor network composed of SnO_2 nanowires. This signal is further amplified by temperature variations across the sensor chip. The *KAMINA*-based E-nose technology leverages temperature and thickness gradients of the gas-permeable MOS coating to distinguish between individual sensing elements laterally. The redox interaction between the analyte molecule and the MOS interfaces, which

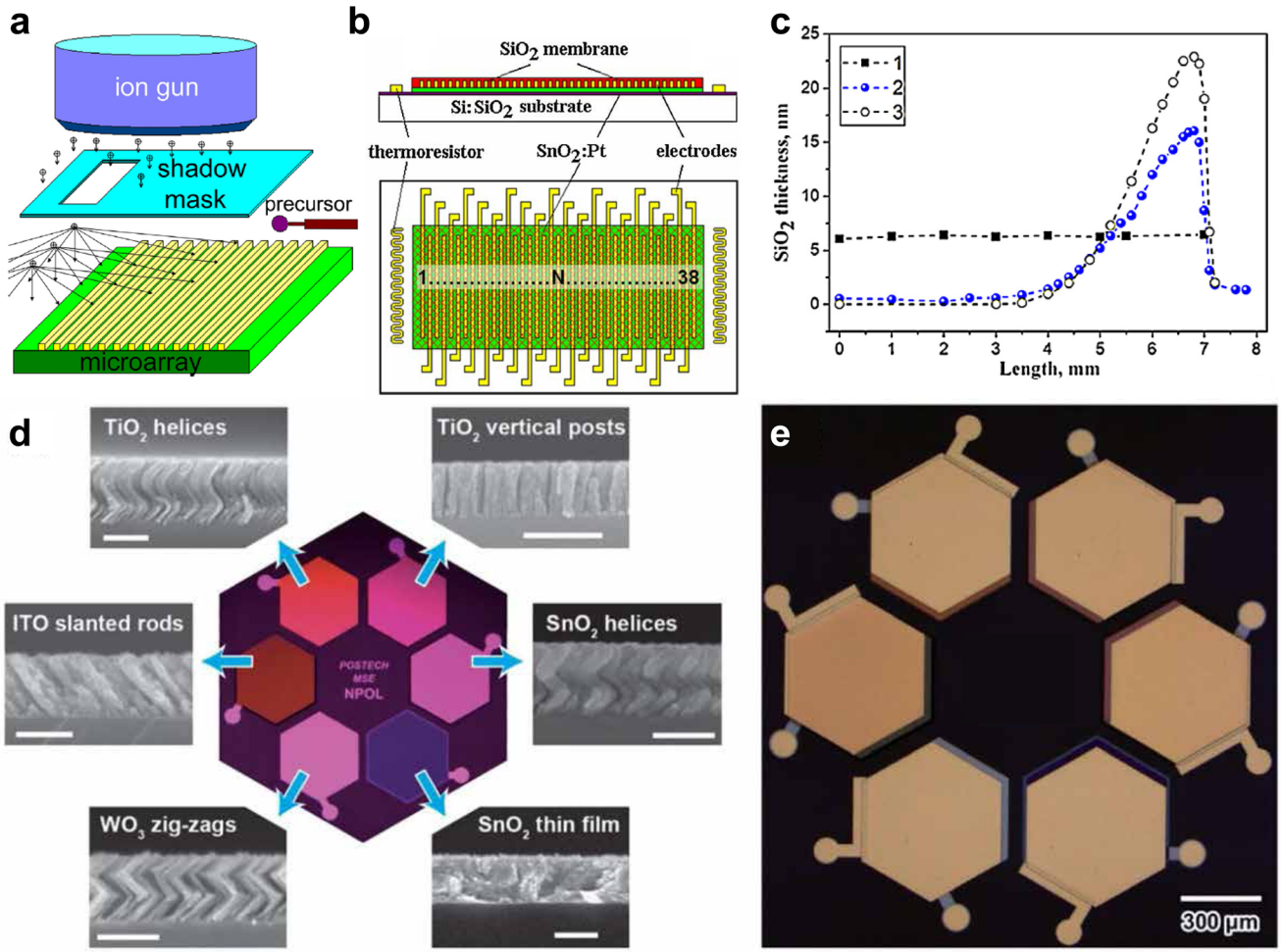

Fig. 3 (a) A schematic illustration of SiO_2 membrane deposition by ion beam assisted chemical deposition (b) an illustration of SiO_2 coating deposition over E-nose (c) the thickness of deposited SiO_2 (d) an optical microscopy image of the prototype E-nose chip after the deposition process for six distinct sensing layers. Accompanying the image are cross-sectional scanning electron microscopy (SEM) images. The scale bars in the images represent a length of 300 nm (e) an optical microscopy image presented here showcases the E-nose after the application of top and pad electrodes on the device illustrated in (d). Reprinted with permission from ref. 61 and 62 with permission from Elsevier, Copyright 2013 and Royal Society of Chemistry, Copyright 2013.

is temperature-dependent, results in gas-specific conductivity patterns. LDA analysis of data from 38 channels confirms that the sensor can clearly differentiate between target gas patterns, thus proving its suitability for gas differentiation. The initial implementation of SnO_2 nanowires in an E-nose that relies on gradient gas sensor arrays was successful. The unique structure of this sensing material maintains high gas permeability even with reduced nanowire diameter. Furthermore, nanowire mats possess a dual signaling mechanism based on permeation and purification. These findings are expected to pave new ways for deliberately regulating the sensitivity and discrimination of various E-noses.

Hwang *et al.* developed a smaller and more cost-effective E-nose using modern microelectronic processes than previous models.[62] The E-nose features ordered nanostructure arrays with excellent position and shape controllability, and reproducibility achieved through oblique angle deposition. By rotating the substrate and adjusting the vapor flux incidence angles, three-dimensional arrays of various nanostructures such as helices, oblique rods, vertical columns, zigzags, and square spirals were fabricated (Fig. 3d and e). The E-nose was integrated using a straightforward and cost-effective method of photolithography, followed by deposition using either an e-beam evaporator or sputter, and then the lift-off method.

The nanostructured MOS created through this method can be annealed into a structure that nearly approaches single crystallinity. The fabricated transparent chemiresistive sensors consist of MOS films with unique nanostructures that exhibit significant long-term stability, high sensitivity, and extremely low power consumption. Ultimately, they integrated six gas sensors made of different MOSs (TiO_2, indium tin oxide [ITO], SnO_2, and WO_2) with different active layer structures (thin film, spiral, vertical column, and zigzag) into a single electronic chip. The SnO_2 nano-gel sensor showed superior sensi-

tivity to all three gas species (CO, NO_2, H_2), with the highest sensitivity noted for NO_2 gas.[62]

However, the sensitivity to CO gas was relatively low, which was attributed to the low operating temperatures. Each gas sensor in the E-nose system exhibited a specific sensitivity pattern for various molecules and could distinguish between different gas types.[62] This versatility allows for the tuning of gas sensitivity, increasing design freedom, and manufacturing E-noses with excellent selectivity, high sensitivity, short response times, low power consumption, long-term stability, and rapid diagnostics. By utilizing state-of-the-art micro-fabrication processes, the integration of gas sensor arrays with other sensors and optoelectronic devices into a single chip can be achieved cost-effectively and conveniently, paving the way for multi-sensor smart chips.

Furthermore, Kim *et al.* developed a highly sensitive and selective breath sensor using hollow apoferritin protein-templated nano-catalysts and electrospun MOS nanostructures.[65] Their goal was to enhance the gas sensing properties by increasing the surface area of the sensing materials through the fabrication of nanostructures and by functionalizing the one-dimensional MOS nanostructures to improve selectivity. The sensor array device consisted of pristine WO_3 nanofibers (NFs), Apo-Pt WO_3 NFs, Apo-PtCo WO_3 NFs, and Apo-PtY WO_3 NFs. These sensors were tested for their ability to detect biomarkers of certain diseases in breath, including hydrogen sulfide (H_2S), acetone, and toluene. It was observed that individual Pt nanoparticles were uniformly immobilized on WO_3 NFs without agglomeration. The resulting sensors exhibited enhanced sensitivity to target gases, with Apo-Pt WO_3 and Apo-PtY WO_3 sensors showing improved sensitivity to acetone compared to pristine WO_3, while Apo-Pd WO_3 was sensitive to toluene. Additionally, Apo-Pt WO_3 and Apo-Rh WO_3 sensors demonstrated increased sensitivity to H_2S.

4.1 Fabrication techniques for MOS-based E-nose systems

The fabrication of MOS-based E-nose systems involves several techniques, both top-down and bottom-up approaches, that enable the synthesis of MOSs with tailored properties, as shown in Fig. 4. Top-down fabrication techniques, which start from bulk materials and work towards the nanoscale, shape materials into desired forms through physical or chemical means. In the context of sensing applications, top-down approaches allow for precise control over the size and shape of nanostructures. However, these methods can introduce defects and imperfections due to the harsh processing conditions often involved, potentially resulting in a lower surface area compared to bottom-up methods, a significant disadvantage for applications relying on surface interactions, such as gas sensing.[66,67]

For instance, sputtering facilitates the creation of uniform thin films, crucial for developing consistent and reliable sensing layers. Despite its precision, sputtering is associated with higher costs and slower production rates.[68]In contrast, mechanical milling offers a more cost-effective alternative for producing nanoparticles, though it provides less control over particle uniformity and risks contamination from the milling process.[69] Chemical etching, another top-down method, is particularly useful for etching specific patterns and shapes at the nanoscale. This technique can create high-surface-area structures beneficial for gas sensing but can be complex and potentially involve hazardous substances. Microwave-assisted techniques, which significantly reduce reaction times, enhance the purity of metal oxide nanoparticles but require specialized equipment and can lead to thermal inconsistencies. Lastly, laser ablation produces high-purity nanoparticles without the need for chemical reactants, thus reducing environmental impact. However, the scalability and cost of this technique remain challenging for mass production.[66,68]

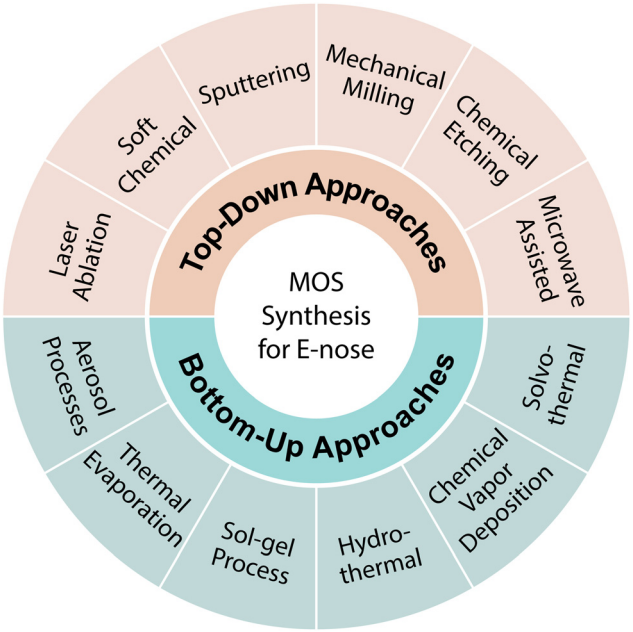

Fig. 4 Fabrication techniques of MOS nanostructures for E-nose systems.

Transitioning from the forceful top-down to the more assembly-oriented bottom-up approaches, the synthesis of MOS for E-noses adopts a different perspective. Bottom-up strategies excel in their precision, creating structures atom by atom and resulting in materials with properties finely tuned to the requirements of gas sensing.[70] These techniques typically produce metal oxides with increased surface area and enhanced chemical functionality, critical attributes for the sensitivity and specificity required in E-nose systems.

This shift from the deconstructive nature of top-down methods to the constructive essence of bottom-up approaches highlights the diverse toolkit available for fabricating advanced sensing materials. As we delve deeper into bottom-up techniques, we aim to illustrate how they complement top-down methods, collectively offering a comprehensive spectrum of options for developing sophisticated metal oxide sensors essential for E-nose operation. These varied fabrication strategies, as depicted in Fig. 4, play a pivotal role in advancing

sensor technology, each contributing unique benefits to the field of gas detection and analysis.

4.1.1 Sol–gel method. The sol–gel method is a versatile fabrication technique for MOSs, offering precise control over the composition, morphology, and porosity of the resulting materials. In this approach, metal alkoxides or salts undergo hydrolysis and condensation to form a sol, which then transitions through gelation and drying processes.[71,72] Achieving uniformity in complex compositions requires meticulous regulation of these reactions, which involve diverse precursors and are modulated through various chemical methods. The adaptability and detailed control afforded by this method make it highly suitable for a range of applications including catalysts, sensors, optics, and energy conversion devices.[73–75]

The sol–gel process is frequently used to produce a diverse array of materials, such as inorganic membranes, monolithic glasses and ceramics, thin films, ultra-fine powders, and hybrid materials.[75] This process begins with the hydrolysis of a precursor solution, which generates colloidal particles that serve as the fundamental building blocks. Subsequent condensation of these particles forms a gel-like substance, which can be further processed into the desired material.

Recently, the sol–gel technique has gained prominence as a promising method for depositing gas sensors.[71] It offers several advantages over other deposition methods, including operation at lower temperatures, high purity of the deposited material, and control over film thickness and porosity. Sol–gel-based gas sensors are now extensively used in various applications such as environmental monitoring, automotive exhaust detection, and medical diagnostics.[75]

MOSs synthesized *via* the sol–gel method have been widely utilized in E-nose systems (Fig. 5a). Using this technique, nanoparticles of TiO_2 doped with chromium (Cr) were effectively synthesized. Subsequently, a hydrogen gas sensor based on Cr-doped TiO_2 was investigated under elevated temperatures. Among various doping concentrations tested, the sensor incorporating 5 atomic percent (at%) chromium-doped TiO_2 exhibited optimal gas sensing performance at 500 °C. Notably, this sensor displayed a response value of 152.65 upon exposure to 1000 parts per million (ppm) of hydrogen, with response and recovery times of 142 seconds and 123 seconds, respectively (Fig. 5b and c).[72]

Similarly, a sol–gel dip coating process was employed to fabricate nano-crystalline thin films of indium oxide (In_2O_3), tin oxide (SnO_2), and tin-doped indium oxide (ITO).[76] The thickness of these films increased with the duration of the dipping time. Remarkably, these sensors showed significant sensitivity to hydrogen sulfide (H_2S) gas when operated at low temperatures and demonstrated a remarkable ability to selectively detect H_2S, with minimal responses to other gases such as liquefied petroleum gas (LPG), carbon dioxide (CO_2), carbon monoxide (CO), ammonia (NH_3), ethanol (C_2H_5OH), and chlorine (Cl_2).

Specifically, the indium oxide sensor exhibited sensitivity toward H_2S gas at a temperature of 115 °C, with response and recovery times ranging from 19 to 26 seconds and 34 to 91

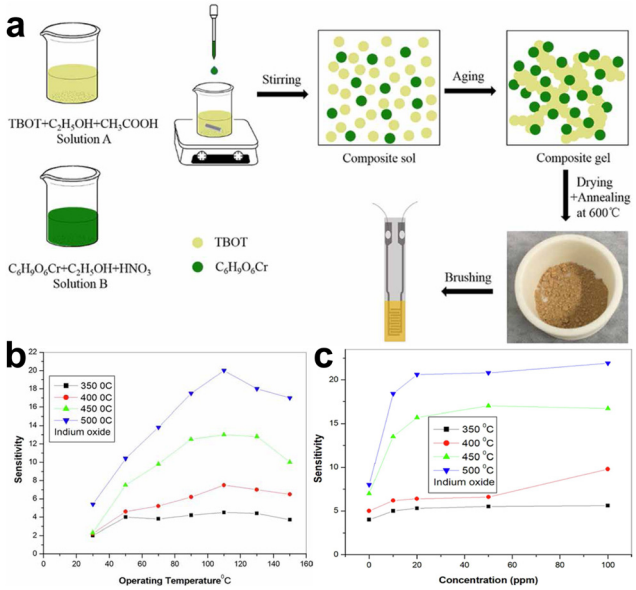

Fig. 5 (a) The schematic illustration of sol–gel steps for both undoped and chromium-doped titanium dioxide nanopowders, along with the assembly of gas sensors. Reprinted with permission from ref. 72. (b) The sensitivity of indium oxide films to 10 ppm of H_2S gas at various operating temperatures, namely 350 °C, 400 °C, 450 °C, and 500 °C, is illustrated. (c) The sensitivity levels of indium oxide films when exposed to varying concentrations of H_2S gas. Reprinted with permission from ref. 76 with permission from Elsevier, Copyright 2023.

seconds, respectively. The SnO_2 sensor responded quickly to 10 ppm of H_2S at 120 °C compared to its recovery times, especially for films synthesized at temperatures of 525 °C, 450 °C, and 350 °C. Notably, the tin oxide film formed at 350 °C showed improved recovery characteristics, although these improvements were temporary. The ITO sensors with 70% tin content exhibited the highest sensitivity to H_2S at 100 °C. Sensors with as low as 40% tin concentration were sensitive to H_2S at 110 °C and 120 °C. Despite their quick response to 25 ppm of H_2S within their respective operating temperatures of 100 °C, 110 °C, and 120 °C, the recovery times for these films were longer than their response times, ranging from 70 to 90 seconds.[76]

4.1.2 Hydrothermal synthesis. Hydrothermal synthesis is a widely employed technique for the fabrication of MOSs, offering remarkable control over the composition, crystallinity, morphology, and properties of the resulting materials.[77] In this process, the reaction occurs in a closed system under high-pressure and elevated-temperature conditions, mimicking the natural hydrothermal environment. The precise manipulation of reaction parameters such as temperature, pressure, pH, and duration allows for the tailored synthesis of MOSs with desired characteristics.[77]

This method enables the formation of well-defined crystalline structures, including nanoparticles, nanowires, and nanosheets, which exhibit enhanced surface area and unique physical and chemical properties. These features render them highly attractive for a diverse range of applications, including

catalysis, energy storage, sensors, and electrochemical devices.[78] Furthermore, the hydrothermal synthesis route offers the advantage of producing MOSs with high purity and homogeneity, facilitating the investigation of their fundamental properties and enabling the exploration of novel functionalities for advanced technological advancements. A schematic illustration of a hydrothermal synthesis for MOS sensing material is shown in Fig. 6a.

The synthesis of MOSs through this method involves a complex series of chemical reactions and nucleation processes, influenced by factors such as precursor concentration, temperature, pressure, and pH. These parameters play a critical role in determining the crystal structure, size, and morphology of the resulting MOSs. The hydrothermal environment provides a conducive setting for the dissolution of precursors, their subsequent diffusion, and the eventual reformation into MOS structures.[79] The high-pressure conditions help suppress undesired side reactions and favor the formation of thermodynamically stable MOS phases.

By meticulously adjusting the hydrothermal parameters, MOS materials can be engineered to possess desired properties such as enhanced electrical conductivity or improved thermal stability. This precision opens up possibilities for innovative functionalities, such as the creation of highly sensitive gas sensors. These advancements hold significant potential for applications in various scientific and technological fields, where sensors could improve pollution monitoring and continuous health monitoring. MOSs synthesized *via* hydrothermal synthesis, such as ZnO and iron oxide (Fe_2O_3),[80,81] have demonstrated remarkable gas-sensing properties.[82] These nanomaterials have been integrated into E-noses for detecting VOCs in the food industry and diagnosing diseases based on breath analysis.

The hydrothermal synthesis of α-Fe_2O_3 microcubes at 160 °C for 12 hours results in well-defined cubic morphologies, as depicted in the SEM and TEM images (Fig. 6b and c, respectively). These images highlight the uniform size and crystalline purity of the microcubes. The selectivity of these microcubes towards various 30 ppm testing gases is demonstrated in Fig. 6d, emphasizing their potential for selective gas detection. Additionally, Fig. 6e shows the response and recovery curves upon exposure to acetone gas, illustrating their effective sensing performance with notable response times and recovery capabilities. Such characteristics underscore the suitability of α-Fe_2O_3 microcubes in applications like environmental monitoring and industrial processes, due to their high sensitivity and selectivity.

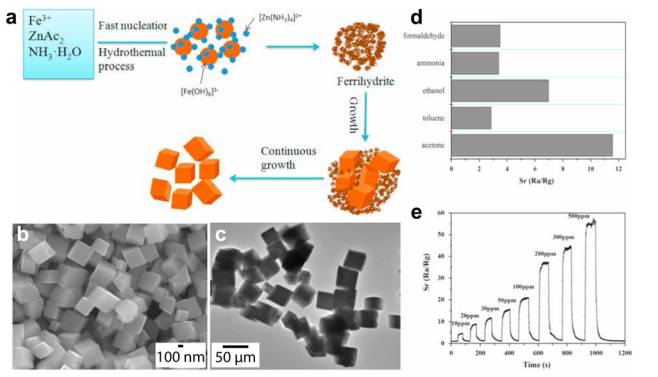

Fig. 6 (a) Schematic illustration of the possible formation process of α-Fe_2O_3 microcubes. (b) SEM image (c) TEM image of as-synthesized α-Fe_2O_3 at 160 °C for 12 h. (d) selectivity of α-Fe_2O_3 microcubes to different 30 ppm testing gases. (e) The response and recovery curves of α-Fe_2O_3 microcubes upon exposure to acetone gas. Reprinted with permission from ref. 81 with permission from Elsevier, Copyright 2015.

A one-step hydrothermal approach was effectively utilized to synthesize tungsten oxide (WO_3) nanofibers, achieving remarkable gas-sensing capabilities, the sensor exhibited a significantly enhanced response to ethanol gas (10–50 ppm), with response values reaching as high as 62 to 100 ppm at a temperature of 350 °C.[82] ZnO nanostructures composed of nanorods, with an average outer diameter of 50 nm and a length of 550 nm, were fabricated using a hydrothermal method assisted by methylamine.[80] The gas-sensing performance of these ZnO nanostructures towards carbon monoxide (CO) at room temperature was found to be selective, with the sensitivity reaching 75%. Furthermore, the response and recovery times for detecting CO gas at concentrations of 2 ppm, 4 ppm, and 6 ppm were 1.7 seconds and 2 seconds, 2 seconds and 3 seconds, and 3 seconds and 4 seconds, respectively.[80]

Through a hydrothermal process, nanocrystalline SnO_2 particles approximately 3.3 ± 0.6 nm in size were successfully synthesized. The presence of chloride ions (Cl^-) during both the synthesis and subsequent thermal treatment stages influenced the atomic ratio of oxygen to tin (O/Sn) in the SnO_2 material. Notably, the gas sensing performance of the as-synthesized SnO_2 sensors was enhanced by subjecting them to a heat treatment at 350 °C for 5 minutes, partially eliminating the chloride ions. As a result, the thermally treated SnO_2 material exhibited exceptional gas-sensing capabilities specifically for alcohol detection (ethanol, methanol, and propanol) at 220 °C, from concentrations of 1.7 to 500 ppm, with a detection limit of approximately 1.7 ppm.[83]

4.1.3 Thermal evaporation. Thermal evaporation synthesis is a widely employed technique for fabricating MOS materials for gas sensing applications.[84] This process involves the controlled vaporization of metal precursors and the deposition of the resulting vapor onto a substrate under carefully regulated temperature and pressure conditions. The thermal evaporation method allows for precise control over deposition parameters, including substrate temperature, evaporation rate, and pressure. These factors directly influence the morphology, composition, and crystallinity of the synthesized MOS films. By fine-tuning these parameters, it is possible to tailor the properties of the MOS materials, such as their surface area, porosity, and sensitivity to specific gas species.[85]

Thermal evaporation synthesis offers several advantages, including its simplicity, scalability, and the ability to produce uniform and high-quality MOS films with controlled thickness and desired microstructures.[85] MOS materials synthesized *via*

thermal evaporation demonstrate exceptional potential for gas-sensing applications. The unique properties of these materials, such as their high surface-to-volume ratio, well-defined crystallinity, and tailored porosity, contribute to their enhanced gas-sensing performance.[86] The precisely controlled thermal evaporation process allows for the synthesis of MOS films with optimized characteristics for gas sensing, including improved sensitivity, selectivity, and response/recovery times.[87]

The specific gas-sensing mechanisms of these MOS materials involve the adsorption and reaction of target gas molecules on the surface of the MOS films, leading to measurable changes in electrical, optical, or mechanical properties. As a powerful tool for the development of advanced MOS gas sensors, thermal evaporation synthesis enables the exploration of novel sensing materials, the optimization of sensor performance, and the realization of highly sensitive and reliable gas sensing devices for various applications, including environmental monitoring, industrial safety, and healthcare.[67,88]

SnO_2, WO_3, and Ga_2O_3 nanowires were successfully synthesized using a vapor transport method, while TeO_2 nanowires were formed through a simple thermal evaporation process in ambient air.[84] For the formation of SnO_2 nanowires, a modified gas evaporation method utilizing a vacuum evaporator was employed to achieve high raw material temperature and precise atmospheric control. By adjusting the heating temperature and atmosphere, thin nanowires with desired properties were obtained.

In the case of SnO_2 nanowires synthesized by vapor transport, doping with Pd resulted in a highly sensitive sensor, particularly at low temperatures, comparable to traditional SnO_2 sensors. Notably, the nanowire-based sensor exhibited faster response and recovery times for H_2 gas compared to a sensor based on the sputtered film, although the sensitivity was slightly lower.[84] Sensors fabricated from SnO_2 nanowires and microwires using modified gas evaporation displayed superior sensitivity to NO_2 compared to sensors based on nanoparticles, despite having a smaller surface-to-volume ratio than the nanoparticle-based sensors. These nanowire-based sensors also exhibited faster response and recovery speeds for NO_2.

Additionally, sensors with a shorter gap length, matching the length of the nanowires, demonstrated superior sensitivity, response, and recovery, underscoring the significance of the electrode-nanowire interface. For WO_3 nanowire sensors, a decrease in nanowire diameter was found to correlate with increased sensitivity to NO_2.[84] The Ga_2O_3 nanowire sensors exhibited satisfactory sensitivity and reversible behavior at relatively low temperatures, ranging from 100 °C to 300 °C.[84] Meanwhile, TeO_2 nanowires were investigated as gas-sensing materials, revealing their p-type semiconductor characteristics. The TeO_2 nanowire-based sensor demonstrated changes in resistance upon exposure to reducing gases (NH_3 and H_2S) and an oxidizing gas (NO_2), with resistance increasing and decreasing, respectively.[84]

4.1.4. Chemical vapor deposition. Chemical Vapor Deposition (CVD) is a highly versatile and widely employed technique for the synthesis of MOS materials, particularly for gas sensing applications. This method involves the controlled deposition of gaseous precursors onto a substrate, where they undergo chemical reactions to form a thin film of the desired MOS.[89] The CVD process offers fine control over the film's composition, morphology, and crystallinity, enabling the fabrication of MOS films with tailored properties. By carefully adjusting process parameters such as temperature, pressure, precursor concentration, and gas flow rates, precise control over the growth kinetics and structure of the MOS film can be achieved.

Moreover, the CVD technique allows for the deposition of MOS films with large surface areas, high purity, and excellent uniformity, which are crucial for optimizing gas sensing performance.[90] The ability to deposit MOSs with controlled nanostructures and porous enhancers through CVD further enhances their gas sensing capabilities, as these features facilitate the adsorption and diffusion of gas molecules, leading to enhanced sensitivity and selectivity.[89]

In the realm of gas sensing, MOS materials synthesized *via* CVD have demonstrated favorable performance due to their unique characteristics. The controlled deposition process enables the precise engineering of MOS films with high surface area-to-volume ratios, tailored crystal structures, and controlled defect densities.[90] These factors play a vital role in the gas sensing mechanisms of MOSs by promoting efficient gas adsorption and reaction.

Additionally, the CVD method enables the incorporation of dopants into the MOS lattice, further enhancing the gas sensing properties. The tunable nature of CVD facilitates the formation of MOS films with optimized surface chemistries, enabling selective detection of target gases. Furthermore, the high-quality films produced by CVD exhibit excellent mechanical and thermal stability, ensuring the long-term reliability and durability of gas sensors.[90]

Recently, a gas sensor utilizing a thin film of $ZnGa_2O_4$ (ZGO) synthesized through the metal–organic chemical vapor deposition (MOCVD) technique was examined across a temperature range of 25 °C to 300 °C. The sensor exhibited a sensitivity of approximately 22.2 when exposed to a concentration of 6.25 ppm of NO, with a response time of 57 seconds. Furthermore, the sensor demonstrated sensitivities of 1.18, 1.27, 1.06, and 1.00 when subjected to NO_2 (500 ppb), SO_2 (125 ppm), CO (125 ppm), and CO_2 (1500 ppm), respectively.[91] Additionally, quasi-1D nano-architectures of Cu_2O or CuO deposited using CVD showed promising gas sensing performance for 10 ppm of acetone and ethanol at an operating temperature of 200 °C.[92]

In another study, the multi-gas sensing properties of 2D α-MoO_{2-x} were investigated using CVD-grown α-MoO_{3-x} films that were subsequently transferred onto different substrates. This transfer process facilitated the fabrication of planar gas sensing devices on various substrates, including flexible and stretchable platforms. The gas sensors based on the transferred 2D α-MoO_{3-x} films exhibited remarkable sensitivity and distinct selectivity towards H_2S and NO_2 at an operating temperature of 250 °C. The minimum detectable limits for H_2S and

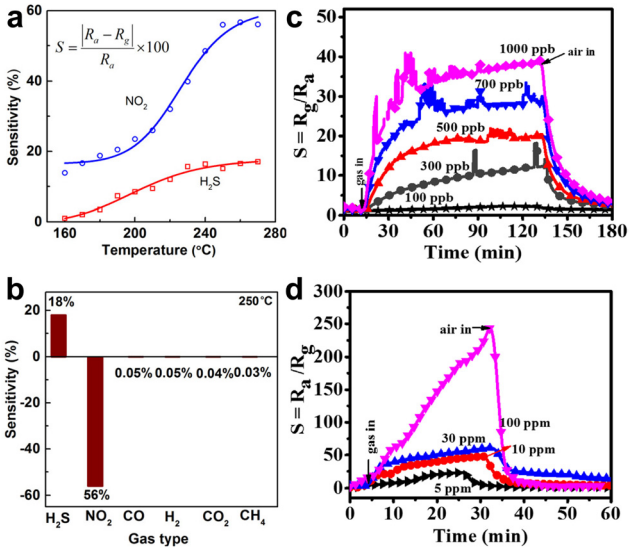

Fig. 7 (a) Sensitivity of the MoO_{3-x}-based sensor upon 300 s of exposure to NO_2 (10 ppm) and H_2S (10 ppm) gases as a function of temperature. (b) Selectivity of the sensors toward different gases upon 300 s of exposure [H_2S (10 ppm), NO_2 (10 ppm), CO (1200 ppm), H_2 (1000 ppm), CO_2 (1000 ppm), and CH_4 (10 000 ppm)]. Reprinted with permission from ref. 93. (c) Responses of ZnO nanoparticulate films for different concentrations of NO_2 at the operating temperature of 225 °C. (d) Response of ZnO films as a function of ethanol concentration at the temperature of 350 °C. Reprinted with permission from ref. 94 with permission from Elsevier, Copyright 2020.

NO_2 were determined to be 1 ppm and 0.5 ppm, respectively. The response and recovery rates for NO_2 were approximately 295.0 and 276.0 kΩ s^{-1}, while those for H_2S were about 28.5 and 48.0 kΩ s^{-1}, respectively. These findings highlight the excellent gas sensing performance of the transferred 2D α-MoO_{3-x} films, emphasizing their potential for highly sensitive and selective detection of H_2S and NO_2 gases (Fig. 7a and b).[93]

4.1.5. Aerosol-assisted chemical vapor deposition. Aerosol-Assisted Chemical Vapor Deposition (AACVD) has emerged as a prominent technique for the fabrication of MOS thin films with tailored properties, particularly for gas sensing applications and sensor arrays. By leveraging the combined advantages of CVD and aerosol processes, AACVD offers fine control over the synthesis of MOS films, enabling the realization of high-performance gas sensors. The process involves the atomization or nebulization of a precursor solution, followed by its mixing with a carrier gas and subsequent transport to a heated reaction chamber.[95] Pyrolysis of the precursor compounds occurs, leading to the controlled decomposition and reaction processes that yield the desired MOS films. The resulting films exhibit desirable characteristics for gas sensing applications, such as high surface area, optimized morphology, and tailored composition, which are crucial for enhanced gas adsorption and response.[95,96]

Thin films prepared by AACVD greatly depend on the growth rate and the precursor concentration. A significant increase in the growth rate, reaching approximately 100 nm min^{-1}, was observed by increasing the precursor concentration in the solution for transparent oxide coatings.[97] These films exhibited excellent electrical properties and achieved a visible light transmission of around 80%, meeting the industrial benchmark for transparent conductive oxide coatings. The AACVD method demonstrated precise control over material doping, allowing for potential high-throughput synthesis of industrially important materials and enabling the utilization of a broader range of precursors and dopants.[98]

Aerosol flow affects the density of nucleation sites and grain size, while temperature significantly influences the morphology of the deposited films. Films grown at temperatures of 350 °C, 375 °C, and 400 °C exhibit preferential orientation along the *c*-axis, with the best degree of preferential orientation observed at 375 °C. The activation energy for the chemical reaction is determined to be 1.06 eV.[99]

The sensing performance of MOS synthesized by AACVD greatly depends on the deposition temperature. Shujah *et al.* demonstrated the synthesis of WO_3 nanostructures *via* AACVD and their application as H_2S gas sensors. The findings highlighted the significant impact of deposition temperature on the sensing performance, with the S-450 sensor exhibiting superior sensitivity due to its improved crystallinity and surface morphology.[100] Two different WO_3 nanostructures, S-425 and S-450, were synthesized at deposition temperatures of 425 °C and 450 °C, respectively. The gas sensing properties of these sensors were investigated by exposing them to varying concentrations of H_2S gas (0–60 ppm) at a low operating temperature of 250 °C and a DC bias of 5 V. The results showed that as the concentration of H_2S gas increased from 0 to 10 ppm, the average resistance of the S-425 and S-450 gas sensors decreased by 96.5% and 97.6%, respectively. The sensing mechanism was attributed to the ionosorption of oxygen species on the WO_3 nanostructured surfaces. The significantly enhanced sensing performance of the S-450 sensor was due to its improved crystallinity and surface morphology, which enhanced the adsorption/desorption kinetics of ions.[100]

AACVD can also be used to create interstitial defects in MOS, which enhance the gas sensing performance of MOS-based sensors.[95,98] ZnO films with nanoparticulate and nanopyramidal structures exhibited favorable gas responses to NO_2 gas.[94] The nanoparticulate films showed a high response of approximately 41 to 1 ppm NO_2, while the nanopyramid-shaped films exhibited a response of around 236 toward 100 ppm ethanol (Fig. 7c and d). The improved sensing performance was attributed to the refined microstructure and the presence of zinc interstitial defects in the ZnO films. The surface-depletion model in ZnO and the chemisorption energies of oxygen molecules on Zn-interstitial-enriched crystal facets were identified as key factors contributing to the enhanced gas response.[94] The findings were supported by density functional theory simulations, which highlighted the promotion of oxygen adsorption and subsequent reaction with ethanol due to the presence of Zn interstitials in the ZnO crystals.

Moreover, AACVD enables the fabrication of sensor arrays, where multiple MOS films with distinct compositions can be deposited on a single substrate.[101] This approach allows for the development of diverse sensing elements within a compact platform, leading to the construction of sensor arrays capable of detecting multiple gases simultaneously. The controlled deposition of MOS films using AACVD ensures the reproducibility and consistency of each sensing element, enabling the creation of well-defined and reliable sensor arrays for applications in environmental monitoring, industrial safety, and health care.[102]

4.2 Transduction principle of MOS-based E-nose systems

Chemiresistive gas sensors based on MOS technology exhibit changes in their native resistance when they interact with the gaseous chemical environment through physical and/or chemical means. Despite their wide usage in various applications, the underlying sensing mechanism of MOS-based gas sensors has not been fully elucidated. The sensing process in MOS gas sensors is a complex phenomenon involving multiple physical and chemical processes.[103,104] These sensors typically consist of a MOS material that changes its electrical conductivity when exposed to specific gases.[105] However, the exact mechanisms governing these conductivity changes, including the interactions between gas molecules and the surface of the MOS, are not yet fully understood.

Furthermore, the gas sensing mechanism is influenced by various external factors, such as temperature,[33] humidity,[106] and the presence of other gases.[107] These external factors can significantly impact the sensor's response and, by extension, the investigation of the underlying sensing mechanism. Additionally, the performance of MOS gas sensors can vary depending on the specific composition, morphology, and size of the MOS material used, further contributing to the complexity of the sensing mechanism.

The interaction between gas molecules and the surface of the MOS, leading to chemical reactions and changes in the sensor's electrical properties, forms an integral part of the sensing mechanism. However, studying these surface processes, including adsorption, desorption, and reaction kinetics, presents challenges in terms of experimental investigation and theoretical modeling. To gain a comprehensive understanding, sophisticated analytical techniques and computational methods such as molecular dynamics (MD), density functional theory (DFT), and machine learning (ML) are being developed and refined.[38,108]

Despite the complexity of the sensing mechanism in MOS gas sensors, the oxygen adsorption and desorption model is currently the most widely accepted theory providing insights into their mechanistic attributes.[109,110] Briefly, when these sensors are exposed to air, oxygen molecules adsorb to the surface of MOS sensing materials. This results in the removal of electrons from the conduction band and the formation of various oxygen species, including O_2^-, O^-, and O^{-2} ions.[111–113] In the case of n-type MOS sensing materials, the formation of ionic oxygen species leads to the creation of electron depletion regions beneath the surface, whereas p-type MOS sensing materials exhibit hole accumulation regions (Fig. 8a–c).[114,115]

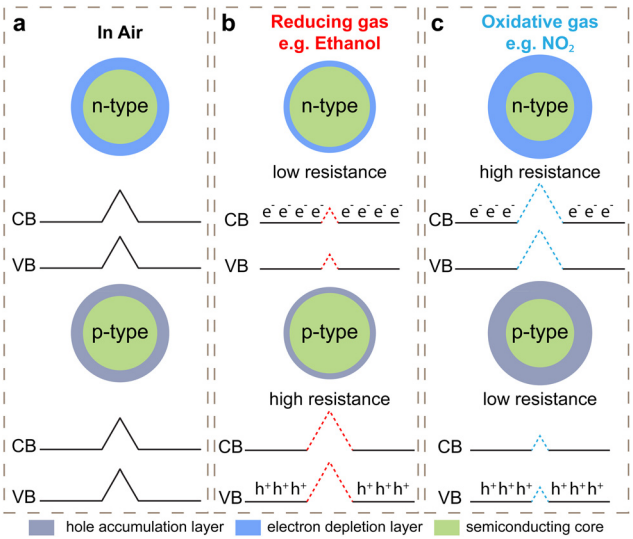

Fig. 8 Schematic illustration of n- and p-type MOS-based gas sensors in the presence of (a) air, (b) a reducing gas such as ethanol, where the resistance of n-type MOSs decreases and that of p-type MOSs increases, and(c) an oxidizing gas such as nitrogen dioxide, where the resistance of n-type MOS increases and that of p-type MOS decreases. Here, CB stands for conduction band and VB stands for valence band.

Different MOS sensing materials demonstrate varying sensing response polarities towards reducing and oxidizing gas analytes. For instance, reducing gases such as hydrogen sulfide (H_2S), hydrogen (H_2), ammonia (NH_3), acetone, and ethanol react with the oxygen ions on the surface of n-type MOS sensing materials. This reaction causes the release of electrons back into the conduction band, resulting in a decrease in the resistance of the sensing material. Conversely, oxidizing gases such as NO_x, N_2O, O_2, and O_3 capture electrons from the oxygen species, leading to an increase in the resistance of the n-type sensing material.[116]

On the other hand, p-type MOS sensing materials act as electron acceptors, and exposure to reducing analytes causes the formation of a thinner hole accumulation region due to the electron–hole recombination process. This reduction in hole concentration increases the overall resistance of p-type MOS. However, the resistance of p-type MOS decreases upon interaction with oxidizing gases.[117]

The performance of chemiresistive gas sensors is influenced by the temperature of the sensing material, particularly its sensitivity. Semiconductors possess specific electrical properties that are intermediate between those of conductors and insulators, and temperature variation significantly affects their conductivity or resistance. At room temperature, conductivity is relatively low but increases as the temperature rises. An intrinsic semiconductor behaves like an insulator at absolute zero, but as the temperature increases, electrons in the valence band become energized and transition to the conduction band, thereby increasing conductivity. Therefore, MOS

chemiresistive gas sensors typically operate at temperatures between 200 and 400 °C.[118–121]

At temperatures below 100 °C, O_2^- ions are prevalent, while temperatures between 100 and 300 °C favor the formation of two equivalents of O^- ions at the MOS–air interface. Above 300 °C, O^- ions reduce back to O_2^- ions. The operating temperature directly influences the charge carrier density at the surface of the sensing material, leading to changes in electrical resistance.[122]

4.3 Advantages of MOS-based E-nose systems for health applications

Chemiresistive MOS-based E-noses offer several advantages for health applications, including:

(a) **Sensitivity and lower limit of detection**: MOS-based E-noses can detect trace amounts of VOCs in the air, making them extremely sensitive to environmental changes. This sensitivity is critical for health applications where minor changes in VOCs can indicate the presence of adverse conditions such as diseases, biofilms, or explosives.

(b) **Portability**: Chemiresistive MOS E-noses are lightweight and portable, making them ideal for use in remote or resource-limited settings. They can be easily transported to different locations and used for on-site testing.

(c) **Non-invasive**: E-noses are non-invasive, requiring no physical contact with the patient. This feature is particularly beneficial for patients sensitive to traditional diagnostic methods.

(d) **Rapid results**: MOS-based E-noses provide results in real time. This rapid analysis can be crucial for quickly diagnosing diseases, monitoring patient health, and tracking disease outbreaks.

(e) **Low cost**: MOS-based E-noses are inexpensive and require minimal maintenance, making them an affordable option for healthcare providers in low-income settings.

5 MOS-based E-nose systems: case studies and applications in healthcare

MOS have gained significant attention and have become one of the most widely studied materials for gas sensing applications in recent years.[4,49] Characterized by their semi-conductive nature, attributed to the incorporation of metal and oxygen atoms within their structural makeup, these materials exhibit unique electrical and surface properties that make them excellent candidates for gas sensing applications.[123] Commonly used MOS materials in gas sensing include, but are not limited to, tin oxide (SnO_2),[124] zinc oxide (ZnO),[108] tungsten oxide (WO_3),[125,126] titanium dioxide (TiO_2),[120] and copper oxide (CuO).[127,128] Additional material examples can be found in other references.[16,110,129]

MOSs can be classified into two main types: n-type and p-type semiconductors,[49] based on their electronic properties. In n-type semiconductors, such as SnO_2, the material possesses an excess of negatively charged electrons, which serve as the majority charge carriers. Conversely, p-type semiconductors, like CuO, exhibit a deficiency of electrons and an excess of positively charged holes, known as electron holes, as the majority of charge carriers.[111] Understanding and controlling these different types of MOSs are essential for tailoring the electrical and gas sensing properties of the materials to suit specific applications.

One of the primary advantages of MOS is their high sensitivity to various gases, especially VOCs and toxic gases, which are of particular interest in healthcare applications.[130] MOS can detect a wide range of gases at low concentrations, enabling their use in the early detection and monitoring of diseases, environmental pollutants, and hazardous gases.[10] The high sensitivity arises from changes in the electrical conductivity or resistance of the MOS material when it interacts with the target gas. This interaction leads to a change in the charge carrier concentration or mobility, resulting in a measurable electrical response.

Another advantage of MOSs is their selectivity. Different MOS materials exhibit varying responses to specific gases, enabling the development of sensor arrays and pattern recognition techniques.[131] By combining multiple MOS sensors, each with distinct selectivity patterns, electronic noses can be created that enable the identification and discrimination of multiple gases simultaneously. This selectivity is based on the unique surface chemistry and reactivity of the MOS, where specific gas molecules form adsorbed species that induce changes in the material's electrical properties.

MOS also offers several practical advantages for gas sensing applications. They are cost-effective, readily available, and can be synthesized using various techniques, such as chemical vapor deposition,[132] sol–gel methods, or sputtering.[119] The fabrication of MOS sensors can be easily integrated into microelectronic circuits, facilitating the development of miniaturized, portable, and low-power gas sensing devices.[126] Additionally, MOS sensors typically operate at moderate temperatures, which makes them compatible with practical applications and reduces power consumption compared to high-temperature sensors.

The surface properties of MOS play a crucial role in their gas sensing performance.[133] The gas-sensing mechanism typically involves the adsorption of gas molecules onto the surface of the MOS, followed by chemical reactions and changes in electrical conductivity. The specific surface area, morphology, and crystal structure of the MOS material significantly influence the gas-sensing properties. High surface area and porous structures provide more active sites for gas adsorption, enhancing sensitivity.[134] The morphology of MOS materials can be tailored to optimize gas–surface interactions and increase the sensor response. Furthermore, the choice of doping elements and their concentration in the MOS can enhance sensing performance by modifying the charge carrier concentration and surface reactivity.[135–137] A summary of recent MOS-based E-noses for various VOCs is presented in Table 2.

Despite their numerous advantages, MOSs also possess certain limitations that should be considered. One such limit-

Table 2 Summary of recent MOS-based E-noses for various VOCs

Sensing material	Structure type	Fabrication technique	Temperature (°C)	VOCs detected	Detection range (ppm)	Data analysis technique	Ref.
Commercial PEN3, CAPINose	TGS sensors	—	RT[a]	Ethanol	10 vol%	Average resistance	45
Thermo-cycled MOS sensors	MOS films	Thermal deposition	260–290	Hexane, butyl acetate	50–175	—	46
Au/SnO_2, Pt/SnO_2, Ni/SnO_2, ITO/SnO_2	Multiplexed nanotube arrays	Spray pyrolysis	RT	Hydrogen, benzene, nitrogen dioxide	50–4000	LVA	57
Pure and Fe-doped In_2O_3	Nanofibers	Electrospinning	250–450	Benzene, xylene, toluene, ethanol, formaldehyde	0.1–1000	PCA	59
TiO_2, SnO_2, ITO, WO_3	Nanorod array	Oblique angle deposition	250	Hydrogen, carbon monoxide, nitrogen dioxide	10–200	—	62
SnO_2	Nanowire gradient	Vapor solid method	326	Isopropyl alcohol, ethanol, carbon monoxide	2–10	LDA	63
Pd/SnO_2	Nanowire sensor array	Vapor solid	150	Isopropyl alcohol	1–50	LDA	64
WO_3	Nanofibers	Electrospinning	350	Hydrogen sulfide, acetone	1–5	PCA	65
Si–SiO_2, Pd–SiO_2, Pt–SiO_2, Ti–SiO_2	Microwire sensor chip	Flexible flame spray pyrolysis	400	Formaldehyde, acetone, ethanol, ammonia	3 ppb	—	131
SnO_2 and WO_3	Villi-like nano structure	Electron beam evaporation	212	Nitrogen oxide, ammonia, ethanol, acetone, toluene, benzene, carbon monoxide	899 ppt–10 ppm	PCA	138
MOS (NiO, CuO, Cr_2O_3, SnO_2 and WO_3)	Nano pattern of multi-array sensing	Lithography	380	Toluene, nitrogen oxide, ammonia, ethanol, acetone, hexane, propanol	5	PCA	139
Cu_2O	Nanospheres	Silanization	180	Ethanol, ethylacetate, toluene, hexane, tetrahydrofuran	25–200	PCA	140
Gold	Nano-islands	*In situ* iterative seeding and growth	RT	Acetone, ethanol, propionaldehyde, acetophenone, benzyl alcohol, benzaldehyde	1–1000	PCA	141
Pt,Pd-doped SnO_2/RGO	Nanohybrids	Hydrothermal	180	Hydrogen, hydrogen sulfide, nitrogen dioxide	0.04–40	PCA, LDA, Hierarchical cluster analysis	142
SnO_2, WO_3, ZnO, In_2O_3	Nanofilms	Screen printing	26–426	Formaldehyde, carbon monoxide, nitrogen dioxide, toluene, ammonia	0.6–1000	—	143
$ZiTiO_3$	Nanoarrays	Hydrothermal, CVD	350	Acetone	1.2–12.5	—	144
Warwick OLFaction (WOLF) E-nose	MEMS MOS-based commercial thick and thin film sensors	—	RT	Acetone, 1-propanol, iso-propanol, iso-butylene	2–10	PCA	145
Pt, Cu, and Ag decorated TiO_2 and ZnO functionalized GaN	Nanowire	Lithography, CVD, Chemical etching	RT	Nitrogen dioxide, sulfur dioxide, hydrogen, ethanol	0.1–10 000	PCA, SVM, k-NN, Decision Tree	146
Au decorated WO_3, SnO_2 and NiO	Thin films, nanostructures	Electron-beam evaporation	100–300	Acetone, toluene, ammonia, hydrogen sulfide	10	PCA	147
Commercial MOS sensors	TGS sensors	—	RT	Ethanol, acetone	—	Partial least squares discriminant analysis	148
Commercial MOS sensors	TGS Sensors	—	RT	Nitrogen dioxide, carbon monoxide	0–50	PCA, C-means clustering, back propagation neural network	149
Reduced graphene oxide	Film	Thermal treatment	200	Formaldehyde, isopropanol, ethanol, acetone, methanol	10–80	PCA, SVM, PCA-SVM	150

Table 2 *(Contd.)*

Sensing material	Structure type	Fabrication technique	Temperature (°C)	VOCs detected	Detection range (ppm)	Data analysis technique	Ref.
Graphene field effect transistor	Film	Chemical vapor deposition	RT	Water, ethanol, methanol	10–90%	Supervised machine learning models	151
SnO_2 and WO_3 particles decorated graphene	Nanoparticles, thin films	Sol–gel	RT–250	Benzene, toluene, xylene	0.2–2	—	152
Graphene sensor array	Thin film	Chemical vapor deposition	RT	Ethanol, hexanal, methyl ethyl ketone, toluene, octane	1–100%	PCA, RF	153
Pd–SnO_2, Pd–WO_3	Nanoflowers, microparticles	Electrohydro dynamic, inkjet printing	100–300	Hydrogen, ammonia, hydrogen-ammonia, ethanol, acetone, ethanol-acetone, toluene, and formaldehyde	3–500	kNN	154
Reduced graphene oxide	film	Metal-ion-induced assembly	RT	Acetone, isoprene, ammonia, hydrothion	0.1–15	PCA	155
SiO_2:In_2O_3, SiO_2:ZnO and SiO_2	Nanofibers	Electrospinning	RT	Ammonia, methylamine, trimethylamine	5–25	PCA	156

[a] RT = room temperature.

ation is their susceptibility to interference from environmental factors, such as humidity and temperature. Changes in humidity levels can affect the surface reactions and the adsorption/desorption processes, leading to variations in sensor response.[106,157] Similarly, temperature fluctuations can influence the electrical conductivity and alter the sensor's baseline. Therefore, appropriate measures and calibration techniques need to be implemented to compensate for these effects.[1]

Another limitation is the potential for cross-sensitivity to multiple gases. While MOS sensors can exhibit selectivity to specific gases, they may also respond to other gases present in the environment. This cross-sensitivity can complicate the interpretation of sensor responses and may require additional data analysis techniques, such as pattern recognition algorithms, to accurately distinguish between different gases.[107] MOSs may also exhibit long-term drift in their sensing performance, leading to reduced stability over time. Factors such as material aging, contamination, and surface poisoning can contribute to this drift and necessitate regular recalibration or replacement of the sensing elements to maintain reliable and accurate measurements.[45,158]

Additionally, MOS sensors typically require elevated operating temperatures (around 200–400 °C) to achieve optimal sensitivity and response.[105] This high-temperature operation can limit their applicability in settings such as portable or wearable devices, where low-power and room-temperature operations are desired. Consequently, efforts are ongoing to develop strategies to lower the operating temperature without sacrificing sensitivity and selectivity. Despite these challenges, ongoing research aims to address these issues and improve the performance of MOS-based gas sensors. By refining material synthesis techniques, exploring advanced sensor architectures, and incorporating innovative signal processing approaches, the limitations of MOSs can be mitigated, further enhancing their potential for various healthcare applications.

6 Applications in healthcare

Traditional methods for disease detection such as chemical analysis of blood, urine, computed tomography (CT), magnetic resonance imaging (MRI), X-ray imaging, and ultrasound can be expensive, invasive, time-consuming, and complex in their use.[159–161] Disease diagnosis through the detection of VOCs in exhaled breath dates back to the early history of medicine.[162,163]

A sample of exhaled breath contains more than ~850 types of VOCs, including both endogenous and exogenous compounds.[164] Major VOCs found in the breath of healthy individuals include acetone (1.2–900 ppb), ethanol (13–1000 ppb), methanol (160–2000 ppb), isoprene (12–580 ppb), and ammonia, with minor components including pentane and higher alcohols, aldehydes, and ketones. The concentration of these VOCs depends on various factors such as diet, lifestyle, environment, and health condition. Thus, the concentration of VOCs varies from person to person.[165,166] The concentration pattern of certain VOCs in the breath has been correlated with the occurrence of specific diseases, also referred to as biomarkers of the disease.

For example, the presence of acetone in the breath has been associated with uncontrolled diabetes.[162] The concentration of VOCs in an exhaled breath ranges from parts per trillion to parts per million. Breath analysis offers several advantages over traditional disease diagnostic methods: it is non-invasive, fast, easy, and does not require skilled medical personnel.[167] Over the past decade, the development of powerful analytical tools such as gas chromatography, infrared spec-

troscopy, and ion mobility spectroscopy[168] has led to increased attention to breath analysis as a tool for early disease detection and continuous monitoring.

An E-nose is a promising technology for detecting VOCs in exhaled breath and offers many advantages over traditional methods, including ease of use, low operational costs, portability, fast response times with rapid results, operation by a non-trained user, and low power consumption.[13,169,170] E-nose technology has already been applied for the early detection of several diseases such as lung cancer, diabetes, breast cancer, and asthma.[171–173] Among various sensing technologies, chemiresistive sensors, particularly those based on metal oxide semiconductor (MOS) nanomaterials, have been the most extensively studied. They are favored mainly due to their high sensitivities to various analytes, ease of fabrication, and short response times.[174,175]

Moon *et al.*[171] fabricated a highly selective and sensitive MOS thin film-based sensor array using photolithography and a dry etching process. The sensor array was able to selectively detect NO, NH_3, and H_2S, which are biomarkers for asthma, kidney disorder, and halitosis respectively, in an environment with 80% relative humidity, similar to the composition of exhaled breath. They constructed a 3 × 3 sensor array composed of different MOS nanostructured thin films including WO_3, SnO_2, and In_2O_3 using e-beam in a glancing angle deposition mode (Fig. 9a).

Sensors with various compositions and morphologies, including thin films, Au-functionalized thin films, and villi-like nanostructures of WO_3, SnO_2, and In_2O_3 with 37% porosity, were fabricated and tested for eight different gases. The sensor array demonstrated very low detection limits, ranging from several hundred parts per trillion to tens of parts per billion.[171] This increase in sensitivity and selectivity was attributed to chemical sensitization and spillover effects due to the functionalization of Au nanoparticles. Moreover, the high porosity increased the surface area, facilitating effective diffusion and adsorption of gas molecules.

The higher porosity enhances the utility factor, leading to improved sensitivity and selectivity.[171] The real-time response of each sensor was recorded in atmospheric conditions with a relative humidity of 80%. The optimal operating temperature was found to be ~168 °C, which is relatively low for MOS-based gas sensors. The sensors showed low responses to hydrocarbon species such as ethanol, benzene, and acetone due to the strong carbon bonds and insufficient thermal energy. The lowest response was observed towards CO_2 due to its centrosymmetric structure.[171] However, Au-functionalized thin films exhibited a significantly high and fast response to 2 ppm of H_2S and 10 ppm of NH_3 at ~168 °C, attributed to the spillover effect (Fig. 9b). To analyze the selectivity of the sensor array, responses from all nine sensors were analyzed using principal component analysis (PCA). As depicted in Fig. 9c and d, PCA clearly distinguished the target vapors of NO, NH_3, and H_2S with a high degree of confidence, using both Au-functionalized and villi-like nanostructures.[171]

Güntner *et al.* developed a portable E-nose for the detection of formaldehyde (FA) in the atmospheric environment, as shown in Fig. 10a.[131] FA is recognized as a potential biomarker

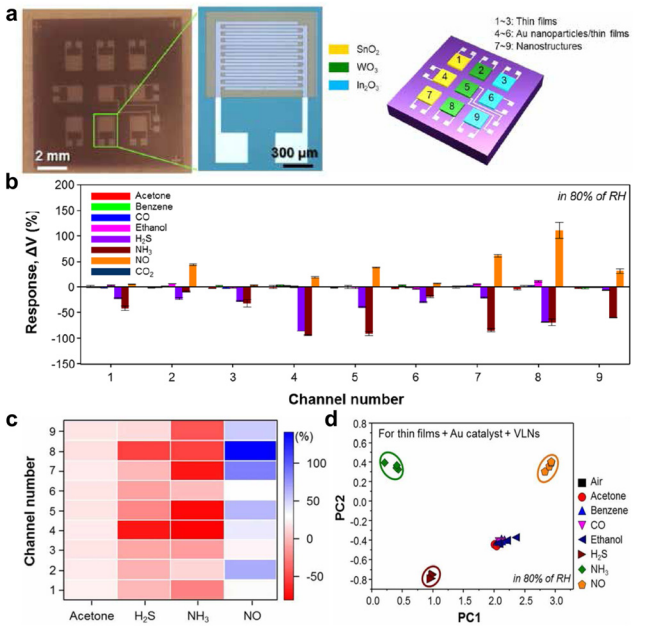

Fig. 9 (a) Optical microscope of the E-nose consisting of 9 sensors based on SnO_2, WO_3, and In_2O_3 deposited on Pt electrodes (b) responses of the E-nose towards various oxidizing and reducing gases in 80% relative humidity (c) color-coded responses of all 9 sensors for acetone, H_2S, NH_3 (d) PCA analysis of the responses from all 9 sensors to recognize the patterns of all gases using thin films + Au-functionalized films + VLNS in 80% relative humidity. Reprinted from ref. 171 with permission from American Chemical Society, Copyright 2016.

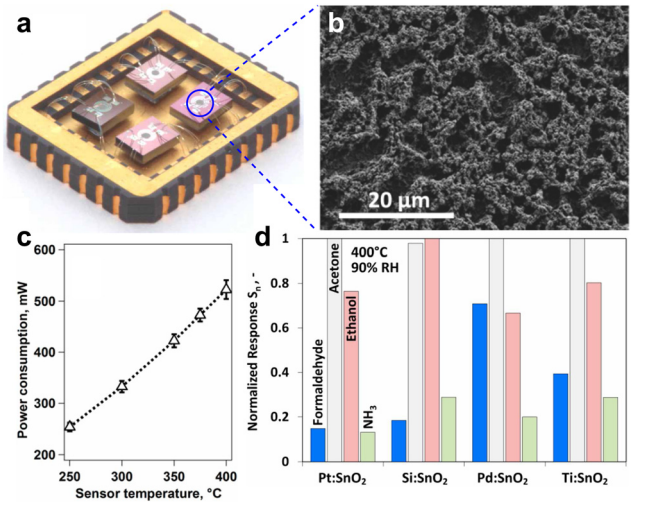

Fig. 10 (a) Four MOS sensors (Pt:, Pd:, Si:, and Ti:SnO_2) wire-bonded to the device package to make an E-nose, suspension of the sensors reduces the heat loss and power consumption (b) highly porous MOS sensing film deposited by flame spray pyrolysis process (c) average power consumption of a single sensor as a function of temperature (d) normalized responses of all 4 sensors to 60 ppb formaldehyde, 600 ppb acetone, 200 ppb ethanol, and 800 ppb NH_3 showing the effect of dopant on the selectivity of each sensor to achieve the cross-reactivity in the E-nose. Reprinted from ref. 131 with permission from American Chemical Society, Copyright 2016.

for lung cancer and a tracer for indoor air quality. For effective medical and indoor air quality monitoring, an E-nose must detect FA below 100 ppb.[131] The device included four highly sensitive and selective films: Pt, Si, Pd, and Ti-doped SnO_2 porous nanostructured films, deposited using flame spray pyrolysis, a facile and scalable technique. The morphology of these films was analyzed by scanning electron microscopy (Fig. 10b).[131]

MOSs typically show improved sensitivity and selectivity at specific temperatures. The optimal temperature for the selective detection of FA was determined to be 400 °C, which is relatively high and could increase the overall power consumption of the E-nose. To mitigate this, the sensor was suspended to decrease power consumption by minimizing heat loss. This adjustment reduced power consumption to 30 mW at 400 °C, making it suitable for integration into battery-powered portable devices (Fig. 10c).

High sensitivity and a low detection limit are essential for detecting lower concentrations of FA in exhaled breath, as compared to the relatively higher concentrations of other gases present. Fig. 10d illustrates the sensing measurements at 400 °C under atmospheric conditions with 90% relative humidity, similar to that of exhaled breath. Various levels of FA concentration (0–180 ppb) were tested, along with realistic interfering levels of acetone, ethanol, and NH_3. The device accurately estimated the entire FA range with an average error of less than 9 ppb in the presence of this four-analyte mixture. The Pd–SnO_2 film exhibited an ultra-low detection limit of 3 ppb and a response time of 140 seconds, attributed to the dopant.[131]

However, a single sensor is not enough to selectively detect such low concentrations of FA due to its poor selectivity. Consequently, a small E-nose comprising four sensors was developed to detect acetone, ethanol, ammonia, and FA in a simulated breath atmosphere. SnO_2 films doped with Pt, Pd, Si, and Ti were utilized. The incorporation of different dopants significantly enhanced the selectivity through the cross-reactivity technique, which is challenging to achieve with a single sensor. Thus, high selectivity can be achieved using an E-nose consisting of four different sensors followed by statistical analysis. This E-nose could be potentially useful in lung cancer screening across broad populations.

Despite the advantages offered by MOS-based sensors operating at optimal temperatures for high sensitivity, the integration of such sensors into wearable E-nose devices presents challenges, particularly due to the high operating temperatures. Safe deployment in wearable devices requires innovative design solutions to ensure user safety and device efficiency. For instance, high-temperature components of the sensor could be insulated and shielded to prevent skin contact, while heat sinks could be utilized to dissipate excess heat. Moreover, the development of low-power heating designs and thermal management systems is crucial for maintaining the sensor's optimal temperature without compromising the comfort and safety of the wearer. Additionally, for reliable operation in diverse environments, the sensor system must be robust against fluctuations in ambient temperature and humidity, achievable through meticulous calibration and environmental compensation techniques.

Recently, an efficient online E-nose-based lung cancer diagnostic method utilizing MOS sensors was proposed and developed.[176] Sixty-five breath samples from lung cancer patients were analyzed and compared with 53 samples from healthy individuals. Various machine learning algorithms were employed, with logistic regression analysis proving to be an adequate data-processing method. The data was classified with 97% accuracy. The performance of this method was promising for general screening purposes, indicating 95% sensitivity and 100% specificity.[176] In another approach, commercial cross-reactive MOS-based sensors were used in an E-nose to discriminate the breath prints of lung cancer patients (six samples) from those of healthy individuals (ten samples) using artificial neural network (ANN) analysis. A sensitivity of 85.7%, a specificity of 100%, and an accuracy of 93.8% were achieved using ANN.[177] Although the MOS-based E-nose demonstrated high accuracy, a larger set of breath samples needs to be tested to confirm the true potential of these devices in a clinical setting.

Kim *et al.*[65] developed an array of sensors based on highly sensitive and selective hollow apoferritin (Apo) protein-templated nanocrystals within one-dimensional chemiresistive MOSs nanostructures to diagnose halitosis through exhaled breath analysis. To enhance the sensitivity, which increases with the surface-to-volume ratio, they significantly enlarged the surface area by fabricating hollow tubular and core–shell MOS structures. To increase the selectivity of the MOS sensors, they were catalytically functionalized with various Apo catalysts including single components (Au, Pt, Pd, Rh, Ag, Ru, Cu, and La) and bimetallic catalysts (PtY and PtCo), as well as the core–shell structure of Au–Pd (Au-core@Pd-shell). A four-sensor array system was developed, consisting of Apo-Pt WO_3 nanofibers (NFs), Apo-Pd WO_3, Apo-Rh WO_3 NFs, and Apo-PtY WO_3. It was tested under a highly humid environment (90% RH) with gas exposures ranging from 1–5 ppm at an operating temperature of 350 °C, as shown in Fig. 11a.[65]

During the sensing characterization, parameters such as sensitivity, selectivity, and limit of detection were analyzed. The focus was on the detection of three main target gases, H_2S, acetone, and toluene, as biomarkers for chronic obstructive pulmonary disease, diabetes, and toluene exposure, respectively. Other gases like hydrogen, ethanol, carbon monoxide, ammonia, methane, pentane, and methyl mercaptan served as interfering gases. Apo-Pt WO_3 and Apo-PtY WO_3 demonstrated higher sensitivity to acetone, a biomarker for diabetes, while Apo-Rh WO_3 exhibited increased sensitivity to H_2S, a biomarker for halitosis, and showed the lowest limit of detection at 0.17 ppb. PCA was performed to evaluate the discrimination capability of the sensors, and biomarkers were distinguished by pattern recognition (Fig. 11b).

To assess the feasibility of the sensor array for breath analysis, the exhaled breath of ten healthy individuals was collected in Tedlar bags, and ten simulated halitosis breath

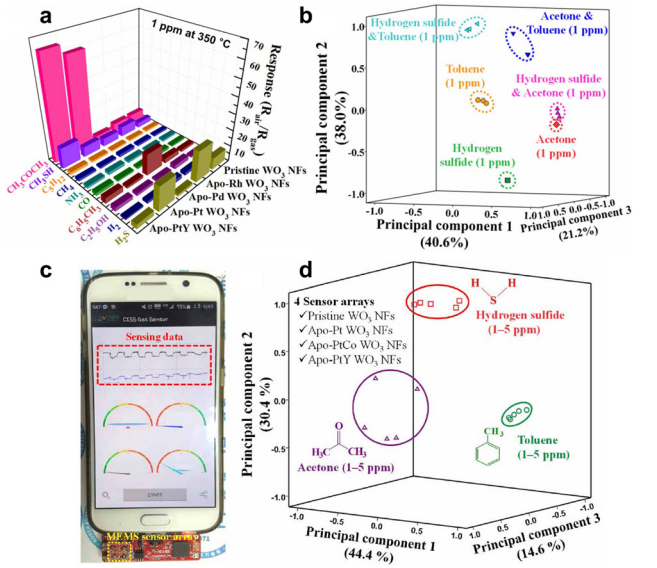

Fig. 11 (a) Sensing responses of WO_3 NF-based films functionalized with various Apo catalysts towards 1 ppm concentration of different biomarkers at 350 °C (b) patterns obtained from PCA for each biomarker in the mixture of biomarkers (c) demonstration of the portability of the E-nose consuming only 2.5–3.5 V of power (d) PCA analysis of the responses showing distinguished clusters (patterns) of acetone, toluene, and H_2S biomarkers. Reprinted from ref. 65 with permission from American Chemical Society, Copyright 2017.

samples were synthesized by maintaining H_2S concentration at 1 ppm, akin to levels found in the breath of halitosis patients.[65] The breath samples were then tested on the four-sensor arrays, which demonstrated a two-fold higher response to the simulated halitosis breath compared to the healthy breath samples, owing to their high sensitivity to H_2S. PCA successfully classified simulated halitosis breath and the breath of healthy individuals into two distinct clusters.

Furthermore, to demonstrate mobile healthcare applications, the sensor array was integrated with a portable diagnostic platform.[65] A key requirement for the portability of the E-nose is low power consumption. To address this, four different sensing layers were prepared: pristine WO_3 nanofibers (NFs), Apo-Pt WO_3, Apo-PtY WO_3, and Apo-PtY WO_3, all mounted on a microelectromechanical systems (MEMS) heating substrate. Fig. 11c displays a sensor module integrated with a smartphone used for gas sensing characterization. Simulated breath samples containing H_2S, acetone, and toluene were injected at 90% RH, and the MEMS heating substrates maintained the operating temperature at 300 °C using voltages ranging from 2.4 to 3.5 volts. Fig. 11d illustrates the results of PCA used to recognize patterns of the three different biomarkers. All simulated breath samples were classified into distinct clusters without overlap.[65] This demonstration of a portable breath analysis platform underscores the potential of MOS-based sensor arrays for rapid monitoring and early diagnosis of diseases.

Given that human breath contains a significant amount of water vapor, it is crucial to perform humidity tests when developing an E-nose for the detection of VOCs in exhaled breath. The sensitivity of MOS-based sensors is highly susceptible to humidity, and given that these sensors typically operate at higher temperatures, maintaining both temperature and humidity at optimal levels during real breath analysis is challenging. Jaeschke *et al.* developed an E-nose equipped with 18 MOS sensors and tested it with six different VOCs (acetaldehyde, acetone, ethanol, ethyl acetate, isoprene, and *n*-pentane) at concentrations ranging from 3 to 18 ppm under both dry and varying humidity conditions.[178] They also studied the drift in sensor response over 20 days, which was corrected using linear discriminant analysis (LDA), partial least squares discriminant analysis (PLSDA), and direct orthogonalization algorithms. The discrimination among VOCs was performed using support vector machine (SVM) and support vector regression (SVR) analyses.[178]

The sensitivity of MOS-based sensors significantly depends on operating temperatures and applied voltages. Real-time breath analysis for the detection and classification of diabetes was performed using a SnO_2 film-based sensor array.[179] A one-dimensional convolutional neural network (CNN) was proposed for classifying diabetic breath samples from those of healthy individuals, with the performance of the algorithm compared to other classification techniques. The proposed model enhanced the classifier and reduced the classification error. In another study, Ping *et al.*[180] employed SnO_2 thin film sensor arrays to detect acetone in exhaled air from 32 volunteers (18 diabetics and 14 non-diabetics), before a meal and at intervals up to two hours post-meal. A 100% discrimination between diabetic and non-diabetic patients was achieved one hour after eating using the SnO_2 films-based E-nose.[180]

Furthermore, MOS-based E-noses can detect and monitor respiratory infectious diseases such as SARS-CoV-2 (COVID-19) and pathogenic bacterial infections through breath analysis.[181–183] A total of 219breath samples were analyzed (57 COVID-19 positive and 162 negative) using a portable, handheld commercial E-nose consisting of three MOS sensors.[181] VOC patterns in the infected and healthy breath samples were distinguished using artificial neural network (ANN) analysis, achieving a sensitivity of 86% and a negative predictive value (NPV) of 0.92. The NPV improved to 0.96 when clinical variables were included in the machine learning multivariate logistic regression analysis.[181] This study underscores the potential of MOS-based E-noses for rapid and early detection of respiratory diseases.

Chernov *et al.* developed a gas analytical system with 14 MOS sensors to detect oncological diseases, including respiratory tract cancer, through exhaled breath analysis.[182] Neural network analysis from the E-nose system demonstrated an accuracy of 81.85% and a sensitivity of 90.73% on real breath samples from patients with various types of oncological diseases. These results were comparable to those from modern high-precision X-ray methods for diagnosing tumors/cancers of the respiratory tract (MRI, CT, PET).[182]

Fiber optic biosniffers for detecting acetaldehyde (AcH) concentrations in breath, associated with various metabolic pro-

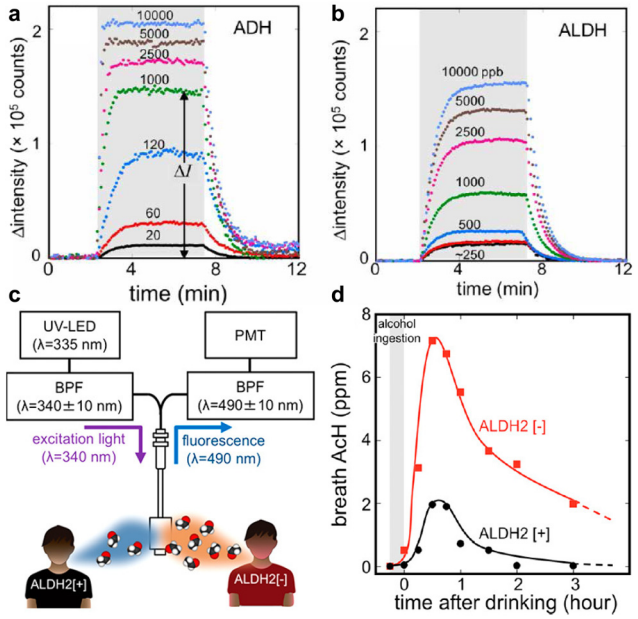

Fig. 12 Responses of (a) ADH-mediated and (b) ALDH-mediated fiber optic biosniffer to different concentrations of AcH. (c) Bifurcated fiber optic biosniffers setup to the ALDH2[+] and ALDH2[−] subjects and (d) their time course of concentration of breath AcH after drinking which is about 3-fold difference at the concentration level. Reprinted from ref. 184 with permission from American Chemical Society, Copyright 2018.

cesses, were characterized by the responses of ADH-mediated and ALDH-mediated biosniffers to different concentrations of AcH, illustrated in Fig. 12a and b respectively.[184] Further, Fig. 12c describes a bifurcated fiber optic biosniffer setup applied to subjects with and without the ALDH2 enzyme. Fig. 12d tracks the time course of breath AcH concentration after alcohol consumption, revealing approximately a 3-fold difference between ALDH2[+] and ALDH2[−] subjects. This technology holds significant potential for personalized healthcare diagnostics, particularly in monitoring metabolic discrepancies related to alcohol consumption.

A hybrid E-nose, comprising an array of organic–inorganic nano-composite gas sensors coupled with three commercial MOS gas sensors, was recently developed to detect complex odors from five different bacterial species (*E. cloacae*, *E. coli*, *P. aeruginosa*, *S. Typhi*, and *S. aureus*).[183] Bacterial samples were controlled at a fixed initial concentration by measuring the optical density at 600 nm of the culture suspensions. A comparative evaluation of the VOCs from five bacterial species grown in Luria–Bertani medium was conducted to identify the optimal incubation time for detecting volatile biomarkers to discriminate among bacteria. Combined with PCA, the E-nose distinguished odors from all bacteria after 6 hours of incubation, capturing 99.7% of the total variance. Table 3 summarizes the detection of different diseases using MOS-based E-noses.

E-nose is an exceptionally beneficial tool, surpassing single gas sensor devices based on MOS nanowires in its capability to detect and differentiate a wide array of gases and VOCs. This versatility makes it suitable for various applications where selective determination of vapor composition is crucial. The scope of E-nose applications includes, but is not limited to, breath testing for preliminary screening, air quality monitoring in various environments such as cities, homes, offices, and factories, explosive detection for defense and surveillance, agricultural and food applications (*e.g.*, assessing food freshness), and water quality testing.

To evaluate the ability to detect *E. coli* in drinking water and prevent waterborne diseases, Carmona *et al.* utilized an E-nose to monitor its growth.[188] The findings showed that the measurements from the E-nose were distinct from those obtained through traditional methods such as pH and optical density measurements. As the bacteria proliferated, the E-nose measurements indicated a drift in the data points over time, reflecting changes in the headspace. In another study, two

Table 3 Summary of use of MOS-based E-noses in disease diagnostics

Diseases	General breath biomarkers	No. of sensors in the E-nose	Human test	Data analysis method	Ref.
Halitosis	Hydrogen sulfide, butyric acid, valeric acid	4	No	PCA	65
Lung cancer	Isoprene, acetone, methanol, benzene, toluene	4	No	Linear regression	131
Halitosis	Hydrogen sulfide, butyric acid, valeric acid	9	No	PCA	171
Asthma	Nitric oxide, pentane, ethane	9	No	PCA	171
Kidney disorder	Ammonia, trimethylamine	9	No	PCA	171
Diabetes	Acetone, acetoacetate, 3-hydroxybutyrate, isopropanol, CO	4	Yes	Convolution Neural Network	179
SARS-CoV-2 (COVID-19)	Ethanol, methanol	3	Yes	Logistic regression analysis	181
Oncological diseases (respiratory tract, lung, larynx cancers)	Formaldehyde, acetaldehyde	14	Yes	ANN, SVM, nearest neighbors method	182
Lung cancer	Isoprene, acetone, methanol, benzene, toluene	32	Yes	PCA, LDA, ANN, KNN, SVM	185
Colorectal cancer	Cyclohexane, methylcyclohexane, 4-methyloctane, hydrogen, methane	10	Yes	PCA and Probabilistic Neural Network	186
Gastric cancer	2-Propenenitrile, furfural, 2-butoxyethanol, hexadecane, nitric oxide	8	Yes	PCA and discriminant factor analysis	187

nanowire-based sensors within the E-nose system were used to detect the presence of *E. coli* and *L. monocytogenes* in potable water.[2,188] The system successfully distinguished both bacteria types, and the PCA plots illustrated the capability to qualitatively monitor bacterial growth over time.

However, the absence of a comparative technique for gauging bacterial concentration did not provide even a qualitative estimate of the limit of detection. In a separate experiment to assess the effectiveness of an E-nose in identifying macrobiotic contamination, the device proved capable of tracking the growth of mold in coffee beans and differentiating various types of spoilage lactic acid bacteria from uncontaminated samples. Furthermore, the system was adept at detecting the presence and proliferation of coliform bacteria in both sewage and well water.

Two types of E-noses were utilized to analyze the breath of smokers and non-smokers: one equipped with six sensors made of WO_3 nanowires, and the other with six commercial SnO_2 sensors. The WO_3 nanowires were synthesized using aerosol-assisted chemical vapor deposition (AACVD). Principal component analysis (PCA) revealed that both E-noses could qualitatively classify the samples from smokers and non-smokers. However, when support vector machines (SVM) were employed to create a confusion matrix, the WO_3 sensor array achieved a success rate of 99.09%, while the SnO_2 sensor array recorded a success rate of 94.59%.[189]

In another application, an E-nose comprising six sensors, including three made of ZnO and SnO_2 nanowires, was used to analyze the growth of skin microbiota in an artificial sweat solution.[190] The system tested three different microbial blends, each containing a bacterium, a yeast, and a fungus, at concentrations of 3.75 and 1.25×10^6 CFU mL^{-1} for prokaryotes and eukaryotes, respectively. The E-nose successfully distinguished a mixture of (*Escherichia coli*, *Rhodotorula* spp., and FGO3), and monitored its development over time, as shown in a 2D PCA plot. The results indicated that the E-nose could differentiate between the microorganism blends based on the VOCs emitted by microbial metabolism. The same group also used a similar setup to detect microbiological pollution in water.[191] By identifying volatiles produced by pathogens such as *Escherichia coli*, *Salmonella typhimurium*, *Vibrio cholerae*, and *Pseudomonas aeruginosa*, including indole, a typical volatile from *E. coli*, the E-nose effectively distinguished potable water from contaminated water.

Zappa *et al.* developed an E-nose equipped with five MOS sensors, including one p-type (NiO) and four n-type (WO_3, SnO_2, ZnO, and Nb_2O_5), to differentiate between pure and contaminated water.[192] The sensors were initially tested individually, and the E-nose was then applied to actual samples of drinking and contaminated water. The device successfully distinguished between the two types of water without prior training, as demonstrated by a PCA plot. Researchers used gas chromatography to identify volatile compounds indicative of macrobiotic growth over a week. Meanwhile, Sonrani *et al.* employed an E-nose with six sensors, some of which were gold-decorated MOS nanowires, to differentiate between potable water, wastewater, and wastewater containing cyanide.[193] The water samples were classified using an artificial neural network (ANN) that had been trained, achieving a classification accuracy of 97.62%. Gas chromatography-mass spectrometry was used to identify the primary volatiles present in the various water samples.

7 Current challenges and future prospects

The evolution of MOS-based gas sensors and E-nose systems over the past three decades has been marked by significant strides, establishing it as a particularly vibrant field within gas sensor research. Innovations have led to significant enhancements in key performance indicators such as sensitivity, selectivity, and response times. Strides have also been made toward achieving efficient operation at lower power levels and even at ambient temperatures.

Despite these advancements, significant hurdles remain. A prominent challenge lies in the accurate detection and quantification of specific analytes within complex chemical mixtures, a common scenario in environments like urban outdoors or in the subtle composition of exhaled breath. Here, single MOS sensors often fall short due to their inability to discriminate among thousands of VOCs, each present at low concentrations. E-noses, with their arrays of sensors, offer a partial solution by generating a distinct pattern that can be associated with a particular analyte or mixture. However, creating a fully reliable E-nose that can consistently recognize and classify such mixtures remains elusive, primarily due to the intricate nature of the chemical interactions at play.

The selection of sensing materials is critical for an E-nose's performance, demanding not only high sensitivity and selectivity but also materials that can quickly respond and recover, remain stable under varying humidity levels, and exhibit distinct selectivity toward individual analytes. Moreover, these materials must maintain consistent performance regardless of environmental conditions and be produced through cost-effective, straightforward fabrication methods. The ultimate choice of sensing material is intrinsically linked to the intended application of the E-nose.

To advance the discrimination capability of E-noses, a broader array of sensors should be integrated, and concerted efforts are necessary to develop more selective sensing materials. This involves extensive research into diverse materials, possibly through the use of heterostructures that combine n-type and p-type semiconductors, and exploring new material engineering techniques to enhance selectivity and pattern recognition efficiency.

Portability is another crucial aspect that differentiates E-noses from traditional VOC detection instruments. For practical adoption in devices like smartphones and wearables, E-noses must be compact, capable of operating at low temperatures to conserve energy, and compatible with high-perform-

ance computing systems. Thus, the quest for nanomaterials that satisfy these conditions is a pivotal research direction.

Furthermore, the long-term stability of sensing materials poses an ongoing challenge. To transition from research prototypes to real-world applications, E-noses require sensors that can sustain prolonged usage without degradation, ideally operating at room temperature with minimal power demands. Focused research on developing such stable sensing materials will be fundamental to the widespread deployment of E-noses in healthcare and beyond.

The trajectory for MOS-based E-noses points towards integrating advanced materials science with sophisticated data analysis algorithms, expanding the realm of machine learning and artificial intelligence in sensor technology. In healthcare, this could translate to non-invasive diagnostics and continuous health monitoring, revolutionizing patient care and disease management. As we navigate these challenges, the concerted efforts of researchers, industry stakeholders, and interdisciplinary collaboration will be paramount in realizing the full potential of E-nose technology in practical, everyday applications.

8 Conclusions

In summary, the E-nose is a promising technology that mimics the mammalian olfactory system to distinguish odors and is already beginning to have an impact on various areas of human life to improve quality of life. Particularly, the food processing industry is increasingly relying on the E-nose to monitor quality and freshness. The demand for the E-nose in healthcare and medical diagnostics has been growing over the years since the discovery of VOCs in exhaled breath. The concentration and nature of theseVOCs depend on the condition of the individual and vary from person to person. VOCs have been strongly correlated to various diseases and are called biomarkers of these diseases.

An E-nose consists of a sensor array and a data acquisition system, which is used for pattern generation and recognition employing ML and ANN techniques. A large number of sensors and a careful selection of sensing materials enable an E-nose to detect and classify different odors into different groups through a pattern recognition system. It can also monitor gases that are explosive or hazardous to humans. A large amount of data is required to develop reliable and efficient E-noses to classify mixtures of odors accurately.

Therefore, the key to developing robust and efficient E-noses is the selection and design of the sensing materials. The diversity of chemiresistive MOS nanomaterials, high sensitivity, and selectivity to a large number of analytes, and fast response times make them the potential sensing materials candidates to develop low-cost and portable E-noses.

In this review, we have examined E-noses based on MOS sensing materials and their applications in crucial aspects of human life to enhance life quality through non-invasive healthcare and early medical diagnostics. MOS-based E-noses are compact, miniaturized, low-cost, and can be operated at low power for practical applications. In healthcare, they are being used to detect lung cancers, breast cancers, diabetes, kidney disorders, and even respiratory and bacterial infections through exhaled breath analysis. There is significant potential for MOS-based E-nose systems to be used in practical applications. However, as scientists become more aware of the requirements and challenges of E-nose systems, current research is increasingly focused on developing E-noses for specific applications. Further investigations and research are essential to developing E-noses with improved performance using MOS nanomaterials to enhance the quality of life. The diversity of MOS nanomaterials could help overcome the shortcomings of E-noses.

Conflicts of interest

There are no conflicts to declare.

Acknowledgements

This research was funded by and has been delivered in partnership with Our Health in Our Hands (OHIOH), a strategic initiative of the Australian National University, which aims to transform healthcare by developing new personalized health technologies and solutions in collaboration with patients, clinicians, and healthcare providers.

References

1 C. Wang, L. Yin, L. Zhang, D. Xiang and R. Gao, *Sensors*, 2010, **10**, 2088–2106.
2 V. Sberveglieri, E. N. Carmona, E. Comini, A. Ponzoni, D. Zappa, O. Pirrotta and A. Pulvirenti, *BioMed Res. Int.*, 2014, **2014**, 1–6.
3 P. Patial and M. Deshwal, *Trans. Electr. Electron. Mater.*, 2021, **23**, 6–18.
4 H. Yu, C. Guo, X. Zhang, Y. Xu, X. Cheng, S. Gao and L. Huo, *Adv. Sustainable Syst.*, 2022, **6**, 2100370.
5 Y.-F. Sun, S.-B. Liu, F.-L. Meng, J.-Y. Liu, Z. Jin, L.-T. Kong and J.-H. Liu, *Sensors*, 2012, **12**, 2610–2631.
6 A. Wilson and M. Baietto, *Sensors*, 2009, **9**, 5099–5148.
7 M. S. Chavali and M. P. Nikolova, *SN Appl. Sci.*, 2019, **1**, 607–637.
8 M. Tonezzer, D. T. T. Le, L. Van Duy, N. D. Hoa, F. Gasperi, N. Van Duy and F. Biasioli, *Nanotechnol. Rev.*, 2022, **11**, 897–925.
9 A. Singh, S. Sikarwar, A. Verma and B. C. Yadav, *Sens. Actuators, A*, 2021, **332**, 113127–113149.
10 E. Comini, *Anal. Chim. Acta*, 2006, **568**, 28–40.
11 L. Zhang and F.-C. Tian, *Anal. Chim. Acta*, 2014, **816**, 8–17.
12 C. Baratto, E. Comini, G. Faglia, G. Sberveglieri, M. Zha and A. Zappettini, *Sens. Actuators, B*, 2005, **109**, 2–6.

13 D. Karakaya, O. Ulucan and M. Turkan, *Int. J. Autom. Comput.*, 2020, **17**, 179–209.
14 L. Capelli, G. Taverna, A. Bellini, L. Eusebio, N. Buffi, M. Lazzeri, G. Guazzoni, G. Bozzini, M. Seveso, A. Mandressi, L. Tidu, F. Grizzi, P. Sardella, G. Latorre, R. Hurle, G. Lughezzani, P. Casale, S. Meregali and S. Sironi, *Sensors*, 2016, **16**, 1708–1731.
15 A. Wilson, *Sensors*, 2013, **13**, 2295–2348.
16 S.-W. Chiu and K.-T. Tang, *Sensors*, 2013, **13**, 14214–14247.
17 A. P. Turner and N. Magan, *Nat. Rev. Microbiol.*, 2004, **2**, 161–166.
18 K. Persaud and G. Dodd, *Nature*, 1982, **299**, 352–355.
19 S. Y. Park, Y. Kim, T. Kim, T. H. Eom, S. Y. Kim and H. W. Jang, *InfoMat*, 2019, **1**, 289–316.
20 M. Tonezzer, L. T. Dang, H. Q. Tran and S. Iannotta, *Sens. Actuators, B*, 2018, **255**, 2785–2793.
21 J. Yan, X. Guo, S. Duan, P. Jia, L. Wang, C. Peng and S. Zhang, *Sensors*, 2015, **15**, 27804–27831.
22 N. J. Pineau, J. F. Kompalla, A. T. Güntner and S. E. Pratsinis, *Microchim. Acta*, 2018, **185**, 1–9.
23 T. I. T. Akamatsu, A. Tsuruta and W. Shin, *Sensors*, 2017, **17**, 1662.
24 E. H. Oh, H. S. Song and T. H. Park, *Enzyme Microb. Technol.*, 2011, **48**, 427–437.
25 W. J. Peveler, M. Yazdani and V. M. Rotello, *ACS Sens.*, 2016, **1**, 1282–1285.
26 K. Arshak, E. Moore, G. Lyons, J. Harris and S. Clifford, *Sens. Rev.*, 2004, **24**, 181–198.
27 P. Raju and Q. Li, *J. Electrochem. Soc.*, 2022, **169**, 057518–057555.
28 R. Johari, U. K. Shambhavi, R. K. Sonker, P. Kumar, R. S. Siddhartha, D. Garg, O. Victor, P. K. Singh, Z. H. Khan and K. Agrahari, in *Perovskite-Based Gas Sensors*, Springer Nature Singapore, 2022, book section ch. 12, pp. 245–259.
29 U. Tisch and H. Haick, *MRS Bull.*, 2010, **35**, 797–803.
30 D. B. Hibbert, *Electroanalysis*, 1998, **10**, 1077–1080.
31 M. Munther, D.-I. Moon, B. Kim, J.-W. Han, K. Davami and M. Meyyappan, *Sens. Actuators, B*, 2019, **299**, 126971–126977.
32 S. M. Scott, D. James and Z. Ali, *Microchim. Acta*, 2006, **156**, 183–207.
33 P. H. Rogers, K. D. Benkstein and S. Semancik, *Anal. Chem.*, 2012, **84**, 9774–9781.
34 K. Shiba, R. Tamura, T. Sugiyama, Y. Kameyama, K. Koda, E. Sakon, K. Minami, H. T. Ngo, G. Imamura, K. Tsuda and G. Yoshikawa, *ACS Sens.*, 2018, **3**, 1592–1600.
35 M. Z. Alom, T. M. Taha, C. Yakopcic, S. Westberg, P. Sidike, M. S. Nasrin, M. Hasan, B. C. Van Essen, A. A. S. Awwal and V. K. Asari, *Electronics*, 2019, **8**, 292–358.
36 V. Schroeder, E. D. Evans, Y.-C. M. Wu, C.-C. A. Voll, B. R. McDonald, S. Savagatrup and T. M. Swager, *ACS Sens.*, 2019, **4**, 2101–2108.
37 S. K. Jha, R. Yadava, K. Hayashi and N. Patel, *Chemom. Intell. Lab. Syst.*, 2019, **185**, 18–31.
38 L. Xu, J. He, S. Duan, X. Wu and Q. Wang, *Sens. Rev.*, 2016, **36**, 207–216.
39 R. K. Sharma, P. C. Chan, Z. Tang, G. Yan, I.-M. Hsing and J. K. Sin, *Sens. Actuators, B*, 2001, **81**, 9–16.
40 R. Ionescu, A. Vancu and A. Tomescu, *Sens. Actuators, B*, 2000, **69**, 283–286.
41 N. Masson, R. Piedrahita and M. Hannigan, *Sens. Actuators, B*, 2015, **208**, 339–345.
42 P. Mielle, *Sens. Actuators, B*, 1996, **34**, 533–538.
43 A. Ziyatdinov, S. Marco, A. Chaudry, K. Persaud, P. Caminal and A. Perera, *Sens. Actuators, B*, 2010, **146**, 460–465.
44 M. Padilla, A. Perera, I. Montoliu, A. Chaudry, K. Persaud and S. Marco, *Chemom. Intell. Lab. Syst.*, 2010, **100**, 28–35.
45 M. Macías, J. Agudo, A. Manso, C. Orellana, H. Velasco and R. Caballero, *Sensors*, 2014, **14**, 10514–10526.
46 M. Bruins, J. W. Gerritsen, W. W. van de Sande, A. van Belkum and A. Bos, *Sens. Actuators, B*, 2013, **188**, 1187–1195.
47 K. H. Baik and S. Jang, *ECS J. Solid State Sci. Technol.*, 2020, **9**, 045010.
48 S. Zanetti, K. Rocha, J. Rodrigues and E. Longo, *Sens. Actuators, B*, 2014, **190**, 40–47.
49 Z. U. Abideen, J.-H. Kim, J.-H. Lee, J.-Y. Kim, A. Mirzaei, H. W. Kim and S. S. Kim, *J. Korean Ceram. Soc.*, 2017, **54**, 366–379.
50 S. Nakagomi, T. Sai and Y. Kokubun, *Sens. Actuators, B*, 2013, **187**, 413–419.
51 L. Zhang and D. Zhang, *IEEE Trans. Instrum. Meas.*, 2015, **64**, 1790–1801.
52 Y. LeCun, Y. Bengio and G. Hinton, *Nature*, 2015, **521**, 436–444.
53 H. Zhang, W. Ye, X. Zhao, R. K. F. Teng and X. Pan, 2018 IEEE International Conference on Electron Devices and Solid State Circuits (EDSSC), 2018, pp. 1–2.
54 Q. Liu, X. Hu, M. Ye, X. Cheng and F. Li, *Int. J. Intell. Syst.*, 2015, **30**, 907–922.
55 M. Shooshtari and A. Salehi, *Sens. Actuators, B*, 2022, **357**, 131418–131429.
56 C. Zang, H. Zhou, K. Ma, Y. Yano, S. Li, H. Yamahara, M. Seki, T. Iizuka and H. Tabata, *Front. Sens.*, 2023, **4**, 1170280–1170288.
57 J. Chen, Z. Chen, F. Boussaid, D. Zhang, X. Pan, H. Zhao, A. Bermak, C.-Y. Tsui, X. Wang and Z. Fan, *ACS Nano*, 2018, **12**, 6079–6088.
58 D. H. Kim, T. H. Kim, W. Sohn, J. M. Suh, Y.-S. Shim, K. C. Kwon, K. Hong, S. Choi, H.-G. Byun, J.-H. Lee and H. W. Jang, *Sens. Actuators, B*, 2018, **274**, 587–594.
59 C.-S. Lee, H.-Y. Li, B.-Y. Kim, Y.-M. Jo, H.-G. Byun, I.-S. Hwang, F. Abdel-Hady, A. A. Wazzan and J.-H. Lee, *Sens. Actuators, B*, 2019, **285**, 193–200.
60 T. H. Kim, A. Hasani, L. V. Quyet, Y. Kim, S. Y. Park, M. G. Lee, W. Sohn, T. P. Nguyen, K. S. Choi, S. Y. Kim and H. W. Jang, *Sens. Actuators, B*, 2019, **286**, 512–520.
61 V. Sysoev, I. Kiselev, V. Trouillet and M. Bruns, *Sens. Actuators, B*, 2013, **185**, 59–69.

62 S. Hwang, H. Kwon, S. Chhajed, J. W. Byon, J. M. Baik, J. Im, S. H. Oh, H. W. Jang, S. J. Yoon and J. K. Kim, *Analyst*, 2013, **138**, 443–450.
63 V. V. Sysoev, J. Goschnick, T. Schneider, E. Strelcov and A. Kolmakov, *Nano Lett.*, 2007, **7**, 3182–3188.
64 V. V. Sysoev, E. Strelcov, M. Sommer, M. Bruns, I. Kiselev, W. Habicht, S. Kar, L. Gregoratti, M. Kiskinova and A. Kolmakov, *ACS Nano*, 2010, **4**, 4487–4494.
65 S.-J. Kim, S.-J. Choi, J.-S. Jang, H.-J. Cho and I.-D. Kim, *Acc. Chem. Res.*, 2017, **50**, 1587–1596.
66 S. T. Bromley, I. d. P. R. Moreira, K. M. Neyman and F. Illas, *Chem. Soc. Rev.*, 2009, **38**, 2657–2670.
67 N. Abid, A. M. Khan, S. Shujait, K. Chaudhary, M. Ikram, M. Imran, J. Haider, M. Khan, Q. Khan and M. Maqbool, *Adv. Colloid Interface Sci.*, 2022, **300**, 102597.
68 A. Biswas, I. S. Bayer, A. S. Biris, T. Wang, E. Dervishi and F. Faupel, *Adv. Colloid Interface Sci.*, 2012, **170**, 2–27.
69 S. Kumar, S. Saralch, U. Jabeen and D. Pathak, *Metal oxides for energy applications*, Elsevier, 2020, pp. 471–504.
70 D. Portehault, F. Gonell and I. Gómez-Recio, *Tailored Functional Oxide Nanomaterials*, 2022, pp. 43–87.
71 A. Adamyan, Z. Adamyan, V. Aroutiounian, A. Arakelyan, K. Touryan and J. Turner, *Int. J. Hydrogen Energy*, 2007, **32**, 4101–4108.
72 L. Xie, Z. Li, L. Sun, B. Dong, Q. Fatima, Z. Wang, Z. Yao and A. A. Haidry, *Front. Mater.*, 2019, **6**, 96–105.
73 J. D. Mackenzie, *J. Non-Cryst. Solids*, 1988, **100**, 162–168.
74 G. J. Owens, R. K. Singh, F. Foroutan, M. Alqaysi, C.-M. Han, C. Mahapatra, H.-W. Kim and J. C. Knowles, *Prog. Mater. Sci.*, 2016, **77**, 1–79.
75 A. Dehghanghadikolaei, J. Ansary and R. Ghoreishi, *Proc. Nat. Res. Soc.*, 2018, **2**, 02008–02029.
76 G. Ramanathan, N. Srinivasan and K. Murali, *Mater. Today: Proc.*, 2023, **92**, 1218–1224.
77 K. Byrappa and T. Adschiri, *Prog. Cryst. Growth Charact. Mater.*, 2007, **53**, 117–166.
78 R. M. Piticescu, R. R. Piticescu, D. Taloi and V. Badilita, *Nanotechnology*, 2003, **14**, 312–317.
79 Y. X. Gan, A. H. Jayatissa, Z. Yu, X. Chen and M. Li, *J. Nanomater.*, 2020, **2020**, 1–3.
80 Vijayakumar, B. Shivaraj, C. Manjunatha, B. Abhishek, G. Nagaraju and P. Panda, *Sens. Int.*, 2020, **1**, 100018–100023.
81 H. Song, Y. Sun and X. Jia, *Ceram. Int.*, 2015, **41**, 13224–13231.
82 S. Cao, C. Zhao, T. Han and L. Peng, *Mater. Lett.*, 2016, **169**, 17–20.
83 H.-C. Chiu and C.-S. Yeh, *J. Phys. Chem. C*, 2007, **111**, 7256–7259.
84 T. Yamazaki, in *Formation of Oxide Nanowires by Thermal Evaporation and Their Application to Gas Sensors*, ed. H. Abbass, InTech, Rijeka, 2011, p. ch. 6.
85 Z. Dai, Z. Pan and Z. Wang, *Adv. Funct. Mater.*, 2003, **13**, 9–24.
86 A. Ponzoni, E. Comini, M. Ferroni and G. Sberveglieri, *Thin Solid Films*, 2005, **490**, 81–85.
87 E. Comini, G. Faglia, M. Ferroni and G. Sberveglieri, *Appl. Phys. A*, 2007, **88**, 45–48.
88 Y. Khan, H. Sadia, S. Z. A. Shah, M. N. Khan, A. A. Shah, N. Ullah, M. F. Ullah, H. Bibi, O. T. Bafakeeh, N. B. Khedher, S. M. Eldin, B. M. Fadhl and M. I. Khan, *Catalysts*, 2022, **12**, 1386.
89 R. Kumar, N. Goel, D. K. Jarwal, Y. Hu, J. Zhang and M. Kumar, *J. Mater. Chem. C*, 2023, **11**, 774–801.
90 S. Vallejos, F. Di Maggio, T. Shujah and C. Blackman, *Chemosensors*, 2016, **4**, 4–22.
91 M.-R. Wu, W.-Z. Li, C.-Y. Tung, C.-Y. Huang, Y.-H. Chiang, P.-L. Liu and R.-H. Horng, *Sci. Rep.*, 2019, **9**, 7459.
92 D. Barreca, E. Comini, A. Gasparotto, C. Maccato, C. Sada, G. Sberveglieri and E. Tondello, *Sens. Actuators, B*, 2009, **141**, 270–275.
93 F. Rahman, A. Zavabeti, M. A. Rahman, A. Arash, A. Mazumder, S. Walia, S. Sriram, M. Bhaskaran and S. Balendhran, *ACS Appl. Mater. Interfaces*, 2019, **11**, 40189–40195.
94 J. Ding, S. Chen, N. Han, Y. Shi, P. Hu, H. Li and J. Wang, *Ceram. Int.*, 2020, **46**, 15152–15158.
95 M. A. Ehsan, S. S. Shah, S. I. Basha, A. S. Hakeem and M. A. Aziz, *Chem. Rec.*, 2022, **22**, e202100278.
96 Z. U. Abideen, W. U. Arifeen and A. Tricoli, *Nanoscale*, 2024, DOI: **10.1039/D4NR00321G**.
97 M. J. Powell, D. B. Potter, R. L. Wilson, J. A. Darr, I. P. Parkin and C. J. Carmalt, *Mater. Des.*, 2017, **129**, 116–124.
98 F. Annanouch, I. Gràcia, E. Figueras, E. Llobet, C. Cané and S. Vallejos, *Sens. Actuators, B*, 2015, **216**, 374–383.
99 S. Sánchez-Martín, S. M. Olaizola, E. Castaño, E. Urionabarrenetxea, G. G. Mandayo and I. Ayerdi, *RSC Adv.*, 2021, **11**, 18493–18499.
100 T. Shujah, M. Ikram, A. R. Butt, M. K. Shahzad, K. Rashid, Q. Zafar and S. Ali, *Nanosci. Nanotechnol. Lett.*, 2019, **11**, 1247–1256.
101 A. S. Mokrushin, Y. M. Gorban, A. A. Averin, P. Y. Gorobtsov, N. P. Simonenko, Y. Y. Lebedinskii, E. P. Simonenko and N. T. Kuznetsov, *Biosensors*, 2023, **13**, 445.
102 X. Hou and K. Choy, *Chem. Vap. Deposition*, 2006, **12**, 583–596.
103 A. Staerz, U. Weimar and N. Barsan, *Sens. Actuators, B*, 2022, **358**, 131531.
104 D. James, S. M. Scott, Z. Ali and W. T. O'Hare, *Microchim. Acta*, 2004, **149**, 1–17.
105 A. Tricoli, M. Righettoni and A. Teleki, *Angew. Chem., Int. Ed.*, 2010, **49**, 7632–7659.
106 C. Sapsanis, H. Omran, V. Chernikova, O. Shekhah, Y. Belmabkhout, U. Buttner, M. Eddaoudi and K. Salama, *Sensors*, 2015, **15**, 18153–18166.
107 K. J. Albert, N. S. Lewis, C. L. Schauer, G. A. Sotzing, S. E. Stitzel, T. P. Vaid and D. R. Walt, *Chem. Rev.*, 2000, **100**, 2595–2626.
108 M. J. Spencer, *Prog. Mater. Sci.*, 2012, **57**, 437–486.
109 P. Rai, S. M. Majhi, Y.-T. Yu and J.-H. Lee, *RSC Adv.*, 2015, **5**, 76229–76248.

110 B. Yang, N. V. Myung and T. Tran, *Adv. Electron. Mater.*, 2021, **7**, 1–37.
111 D. Degler, U. Weimar and N. Barsan, *ACS Sens.*, 2019, **4**, 2228–2249.
112 H. Ji, W. Zeng and Y. Li, *Nanoscale*, 2019, **11**, 22664–22684.
113 M. Chen, Z. Wang, D. Han, F. Gu and G. Guo, *Sens. Actuators, B*, 2011, **157**, 565–574.
114 S. Bai, S. Chen, L. Chen, K. Zhang, R. Luo, D. Li and C. C. Liu, *Sens. Actuators, B*, 2012, **174**, 51–58.
115 C. M. Hung, D. T. T. Le and N. Van Hieu, *J. Sci.: Adv. Mater. Devices*, 2017, **2**, 263–285.
116 M. Kaur, S. Kailasaganapathi, N. Ramgir, N. Datta, S. Kumar, A. Debnath, D. Aswal and S. Gupta, *Appl. Surf. Sci.*, 2017, **394**, 258–266.
117 Y. Kwon, H. Kim, S. Lee, I.-J. Chin, T.-Y. Seong, W. I. Lee and C. Lee, *Sens. Actuators, B*, 2012, **173**, 441–446.
118 Z. Li, Y. Huang, S. Zhang, W. Chen, Z. Kuang, D. Ao, W. Liu and Y. Fu, *J. Hazard. Mater.*, 2015, **300**, 167–174.
119 C. Cantalini, W. Wlodarski, Y. Li, M. Passacantando, S. Santucci, E. Comini, G. Faglia and G. Sberveglieri, *Sens. Actuators, B*, 2000, **64**, 182–188.
120 J. Moon, J.-A. Park, S.-J. Lee, T. Zyung and I.-D. Kim, *Sens. Actuators, B*, 2010, **149**, 301–305.
121 Y.-T. Yu, S. M. Majhi and H.-G. Song, *Procedia Eng.*, 2016, **168**, 227–230.
122 W. Lu, D. Ding, Q. Xue, Y. Du, Y. Xiong, J. Zhang, X. Pan and W. Xing, *Sens. Actuators, B*, 2018, **254**, 393–401.
123 Z. U. Abideen, J.-G. Choi, J. A. Yuwono, W.-J. Lee, K. Murugappan, P. V. Kumar, D. R. Nisbet, T. Tran-Phu, M.-H. Yoon and A. Tricoli, *ACS Appl. Mater. Interfaces*, 2023, **15**, 56464–56477.
124 I. Sayago, M. Aleixandre and J. P. Santos, *Biosensors*, 2019, **9**, 21–33.
125 M. Righettoni, A. Tricoli and S. E. Pratsinis, *Anal. Chem.*, 2010, **82**, 3581–3587.
126 M. Righettoni, A. Tricoli, S. Gass, A. Schmid, A. Amann and S. E. Pratsinis, *Anal. Chim. Acta*, 2012, **738**, 69–75.
127 U. T. Nakate, P. Patil, S.-I. Na, Y. Yu, E.-k. Suh and Y.-B. Hahn, *Colloids Surf., A*, 2021, **612**, 125962–125970.
128 A. Rydosz, *Coatings*, 2018, **8**, 425–444.
129 A. Dey, *Mater. Sci. Eng., B*, 2018, **229**, 206–217.
130 S. Acharyya, S. Nag, S. Kimbahune, A. Ghose, A. Pal and P. K. Guha, *ACS Sens.*, 2021, **6**, 2218–2224.
131 A. T. Güntner, V. Koren, K. Chikkadi, M. Righettoni and S. E. Pratsinis, *ACS Sens.*, 2016, **1**, 528–535.
132 N. Weidler, J. Schuch, F. Knaus, P. Stenner, S. Hoch, A. Maljusch, R. Schäfer, B. Kaiser and W. Jaegermann, *J. Phys. Chem. C*, 2017, **121**, 6455–6463.
133 M. Batzill and U. Diebold, *Phys. Chem. Chem. Phys.*, 2007, **9**, 2307–2318.
134 Z. U. Abideen, J. Choi, J. A. Yuwono, A. Kiy, P. V. Kumar, K. Murugappan, W. Lee, P. Kluth, D. R. Nisbet, T. Tran-Phu, M. Yoon and A. Tricoli, *Adv. Electron. Mater.*, 2023, **9**, 2200905–2200921.
135 Z. U. Abideen, J. Y. Park, H. W. Kim and S. S. Kim, *Nanotechnology*, 2017, **28**, 035501–035512.
136 Z. U. Abideen, J.-H. Kim, A. Mirzaei, H. W. Kim and S. S. Kim, *Sens. Actuators, B*, 2018, **255**, 1884–1896.
137 Z. U. Abideen, J.-H. Kim and S. S. Kim, *Sens. Actuators, B*, 2017, **238**, 374–380.
138 H. G. Moon, Y. Jung, S. D. Han, Y.-S. Shim, W.-S. Jung, T. Lee, S. Lee, J. H. Park, S.-H. Baek, J.-S. Kim, H.-H. Park, C. Kim and C.-Y. Kang, *Sens. Actuators, B*, 2018, **257**, 295–302.
139 H. Kang, S. Cho, J. Ryu, J. Choi, H. Ahn, H. Joo and H. Jung, *Adv. Funct. Mater.*, 2020, **30**, 2002486–2002495.
140 B. Liu, X. Wu, K. W. L. Kam, W.-F. Cheung and B. Zheng, *ACS Sens.*, 2019, **4**, 3051–3055.
141 P. Gupta, H. G. Derami, D. Mehta, H. Yilmaz, S. Chakrabartty, B. Raman and S. Singamaneni, *ACS Appl. Mater. Interfaces*, 2022, **14**, 3207–3217.
142 B. Bhangare, K. Sinju, N. S. Ramgir, S. Gosavi and A. Debnath, *Mater. Sci. Semicond. Process.*, 2022, **147**, 106706–106715.
143 G. Zhang, C. Xie, S. Zhang, J. Zhao, T. Lei and D. Zeng, *ACS Comb. Sci.*, 2014, **16**, 459–465.
144 S. S. A. A. H. Rashid, Y. M. Sabri, A. E. Kandjani, C. J. Harrison, R. K. C. Balasubramanyam, E. D. Gaspera, M. R. Field, S. K. Bhargava, A. Tricoli, W. Wlodarski and S. J. Ippolito, *ACS Appl. Mater. Interfaces*, 2019, **11**, 29255–29267.
145 A. Tiele, A. Wicaksono, S. K. Ayyala and J. A. Covington, *Electronics*, 2020, **9**, 84–100.
146 M. A. H. Khan, B. Thomson, R. Debnath, A. Motayed and M. V. Rao, *IEEE Sens. J.*, 2020, **20**, 6020–6028.
147 J. Lee, Y. Jung, S.-H. Sung, G. Lee, J. Kim, J. Seong, Y.-S. Shim, S. C. Jun and S. Jeon, *J. Mater. Chem. A*, 2021, **9**, 1159–1167.
148 J. Palacín, D. Martínez, E. Clotet, T. Pallejà, J. Burgués, J. Fonollosa, A. Pardo and S. Marco, *Sensors*, 2019, **19**, 1957–1973.
149 J. Chu, W. Li, X. Yang, Y. Wu, D. Wang, A. Yang, H. Yuan, X. Wang, Y. Li and M. Rong, *Sens. Actuators, B*, 2021, **329**, 129090–129100.
150 T. Lu, A. Al-Hamry, J. M. Rosolen, Z. Hu, J. Hao, Y. Wang, A. Adiraju, T. Yu, E. Y. Matsubara and O. Kanoun, *Chemosensors*, 2021, **9**, 360.
151 T. Hayasaka, A. Lin, V. C. Copa, L. P. Lopez, R. A. Loberternos, L. I. M. Ballesteros, Y. Kubota, Y. Liu, A. A. Salvador and L. Lin, *Microsyst. Nanoeng.*, 2020, **6**, 50.
152 S. Behi, N. Bohli, J. Casanova-Cháfer, E. Llobet and A. Abdelghani, *Sensors*, 2020, **20**, 3413.
153 N. S. S. Capman, X. V. Zhen, J. T. Nelson, V. R. S. K. Chaganti, R. C. Finc, M. J. Lyden, T. L. Williams, M. Freking, G. J. Sherwood, P. Bühlmann, C. J. Hogan and S. J. Koester, *ACS Nano*, 2022, **16**, 19567–19583.
154 Z. Li, J. Yu, D. Dong, G. Yao, G. Wei, A. He, H. Wu, H. Zhu, Z. Huang and Z. Tang, *Sens. Actuators, B*, 2023, **380**, 133289.
155 Q. Chen, Z. Chen, D. Liu, Z. He and J. Wu, *ACS Appl. Mater. Interfaces*, 2020, **12**, 17713–17724.

156 R. S. Andre, M. H. Facure, L. A. Mercante and D. S. Correa, *Sens. Actuators, B*, 2022, **353**, 131114.
157 X.-J. Xie, R.-J. Si, J. Zheng, K. Wei, X.-Y. Zheng, C. Chen and C.-C. Wang, *J. Alloys Compd.*, 2021, **879**, 160487–160494.
158 A. Tricoli, M. Graf and S. E. Pratsinis, *Adv. Funct. Mater.*, 2008, **18**, 1969–1976.
159 B. Hochhegger, E. Marchiori, O. Sedlaczek, K. Irion, C. P. Heussel, S. Ley, J. Ley-Zaporozhan, A. S. Souza and H.-U. Kauczor, *Br. J. Radiol.*, 2011, **84**, 661–668.
160 S. Brandman and J. P. Ko, *J. Thorac. Imaging*, 2011, **26**, 90–105.
161 J. Todd and E. E. McGrath, *QJM*, 2010, **104**, 903–904.
162 R. D. Stewart, E. A. Boettner and B. T. Stubbs, *Nature*, 1961, **191**, 1008–1008.
163 R. D. Stewart and E. A. Boettner, *N. Engl. J. Med.*, 1964, **270**, 1035–1038.
164 A. Amann, B. d. L. Costello, W. Miekisch, J. Schubert, B. Buszewski, J. Pleil, N. Ratcliffe and T. Risby, *J. Breath Res.*, 2014, **8**, 034001.
165 J. D. Fenske and S. E. Paulson, *J. Air Waste Manage. Assoc.*, 1999, **49**, 594–598.
166 A. H. Jalal, F. Alam, S. Roychoudhury, Y. Umasankar, N. Pala and S. Bhansali, *ACS Sens.*, 2018, **3**, 1246–1263.
167 A. Tricoli, N. Nasiri and S. De, *Adv. Funct. Mater.*, 2017, **27**, 1605271.
168 F. Röck, N. Barsan and U. Weimar, *Chem. Rev.*, 2008, **108**, 705–725.
169 B. Swanson, L. Fogg, W. Julion and M. T. Arrieta, *J. Assoc. Nurses AIDS Care*, 2020, **31**, 71–79.
170 M. V. Farraia, J. C. Rufo, I. Paciência, F. Mendes, L. Delgado and A. Moreira, *Porto Biomed. J.*, 2019, **4**, e42–e55.
171 H. G. Moon, Y. Jung, S. D. Han, Y.-S. Shim, B. Shin, T. Lee, J.-S. Kim, S. Lee, S. C. Jun, H.-H. Park, C. Kim and C.-Y. Kang, *ACS Appl. Mater. Interfaces*, 2016, **8**, 20969–20976.
172 B. Behera, R. Joshi, G. K. A. Vishnu, S. Bhalerao and H. J. Pandya, *J. Breath Res.*, 2019, **13**, 024001.
173 P. Makaram, D. Owens and J. Aceros, *Diagnostics*, 2014, **4**, 27–46.
174 H. Chen, R. Bo, A. Shrestha, B. Xin, N. Nasiri, J. Zhou, I. Di Bernardo, A. Dodd, M. Saunders, J. Lipton-Duffin, T. White, T. Tsuzuki and A. Tricoli, *Adv. Opt. Mater.*, 2018, **6**, 1800677.
175 A. Tricoli, *Biosensors*, 2012, **2**, 221–233.
176 A. Kononov, B. Korotetsky, I. Jahatspanian, A. Gubal, A. Vasiliev, A. Arsenjev, A. Nefedov, A. Barchuk, I. Gorbunov, K. Kozyrev, A. Rassadina, E. Iakovleva, M. Sillanpää, Z. Safaei, N. Ivanenko, N. Stolyarova, V. Chuchina and A. Ganeev, *J. Breath Res.*, 2019, **14**, 016004.
177 D. Marzorati, L. Mainardi, G. Sedda, R. Gasparri, L. Spaggiari and P. Cerveri, 2019 41st Annual International Conference of the IEEE Engineering in Medicine and Biology Society (EMBC), 2019, pp. 1584–1587.
178 C. Jaeschke, J. Glöckler, M. Padilla, J. Mitrovics and B. Mizaikoff, *Anal. Methods*, 2020, **12**, 4724–4733.
179 S. Lekha and M. Suchetha, *IEEE J. Biomed. Health Inform.*, 2017, **22**, 1630–1636.
180 W. Ping, T. Yi, X. Haibao and S. Farong, *Biosens. Bioelectron.*, 1997, **12**, 1031–1036.
181 A. G. W. E. Wintjens, K. F. H. Hintzen, S. M. E. Engelen, T. Lubbers, P. H. M. Savelkoul, G. Wesseling, J. A. M. van der Palen and N. D. Bouvy, *Surg. Endosc.*, 2021, **35**, 6671–6678.
182 V. I. Chernov, E. L. Choynzonov, D. E. Kulbakin, E. V. Obkhodskaya, A. V. Obkhodskiy, A. S. Popov, V. I. Sachkov and A. S. Sachkova, *Diagnostics*, 2020, **10**, 677.
183 T. Seesaard, C. Thippakorn, T. Kerdcharoen and S. Kladsomboon, *Anal. Methods*, 2020, **12**, 5671–5683.
184 K. Iitani, P.-J. Chien, T. Suzuki, K. Toma, T. Arakawa, Y. Iwasaki and K. Mitsubayashi, *ACS Sens.*, 2018, **3**, 425–431.
185 R. Thriumani, A. Zakaria, Y. Z. H.-Y. Hashim, A. I. Jeffree, K. M. Helmy, L. M. Kamarudin, M. I. Omar, A. Y. M. Shakaff, A. H. Adom and K. C. Persaud, *BMC Cancer*, 2018, **18**, 1–17.
186 D. F. Altomare, F. Porcelli, A. Picciariello, M. Pinto, M. Di Lena, O. C. Lambrenghi, I. Ugenti, A. Guglielmi, L. Vincenti and G. De Gennaro, *Tech. Coloproctol.*, 2016, **20**, 405–409.
187 H. Amal, M. Leja, K. Funka, R. Skapars, A. Sivins, G. Ancans, I. Liepniece-Karele, I. Kikuste, I. Lasina and H. Haick, *Gut*, 2016, **65**, 400–407.
188 E. N. Carmona, V. Sberveglieri, E. Comini, D. Zappa and A. Pulvirenti, *Procedia Eng.*, 2014, **87**, 1453–1456.
189 T. Saidi, T. G. Welearegay, O. Zaim, O. G. Leon, R. Ionescu, N. El Bari and B. Bouchikhi, 2017 ISOCS/IEEE International Symposium on Olfaction and Electronic Nose (ISOEN), 2017, pp. 1–3.
190 E. Carmona, V. Sberveglieri, A. Ponzoni, V. Galstyan, D. Zappa, A. Pulvirenti and E. Comini, *Sens. Actuators, B*, 2017, **238**, 1224–1230.
191 M. Soprani, A. Ponzoni, V. Sberveglieri, E. N. Carmona, M. P. Bhandari, G. Betto and G. Sberveglieri, 2017 ISOCS/IEEE International Symposium on Olfaction and Electronic Nose (ISOEN), 2017, pp. 1–3.
192 D. Zappa, A. Bertuna, E. Comini, N. Kaur, N. Poli, V. Sberveglieri and G. Sberveglieri, *Beilstein J. Nanotechnol.*, 2017, **8**, 1205–1217.
193 M. Sonrani, M. Abbatangelo, E. Carmona, G. Duina, M. Malgaretti, E. Comini, V. Sberveglieri, M. P. Bhandari, D. Bolpagni and G. Sberveglieri, 2018 Workshop on Metrology for Industry 4.0 and IoT, 2018, pp. 68–71.